Drosophila Sirt2/mammalian SIRT3 deacetylates ATP synthase β and regulates complex V activity

Motiur Rahman,[1,2] Niraj K. Nirala,[1,2] Alka Singh,[1,2] Lihua Julie Zhu,[1,2,3] Kaori Taguchi,[5] Takeshi Bamba,[5] Eiichiro Fukusaki,[5] Leslie M. Shaw,[4] David G. Lambright,[2] Jairaj K. Acharya,[6] and Usha R. Acharya[1,2]

[1]Program in Gene Function and Expression, [2]Program in Molecular Medicine, [3]Program in Bioinformatics and Integrative Biology, and [4]Department of Cancer Biology, University of Massachusetts Medical School, Worcester, MA 01605
[5]Department of Biotechnology, Graduate School of Engineering, Osaka University, Osaka 565-0871, Japan
[6]Laboratory of Cell and Developmental Signaling, National Cancer Institute, Frederick, MD 21702

Adenosine triphosphate (ATP) synthase β, the catalytic subunit of mitochondrial complex V, synthesizes ATP. We show that ATP synthase β is deacetylated by a human nicotinamide adenine dinucleotide (NAD^+)–dependent protein deacetylase, sirtuin 3, and its *Drosophila melanogaster* homologue, dSirt2. *dsirt2* mutant flies displayed increased acetylation of specific Lys residues in ATP synthase β and decreased complex V activity. Overexpression of dSirt2 increased complex V activity. Substitution of Lys 259 and Lys 480 with Arg in human ATP synthase β, mimicking deacetylation, increased complex V activity, whereas substitution with Gln, mimicking acetylation, decreased activity. Mass spectrometry and proteomic experiments from wild-type and *dsirt2* mitochondria identified the *Drosophila* mitochondrial acetylome and revealed dSirt2 as an important regulator of mitochondrial energy metabolism. Additionally, we unravel a ceramide–NAD^+–sirtuin axis wherein increased ceramide, a sphingolipid known to induce stress responses, resulted in depletion of NAD^+ and consequent decrease in sirtuin activity. These results provide insight into sirtuin-mediated regulation of complex V and reveal a novel link between ceramide and *Drosophila* acetylome.

Introduction

Mitochondria generate cellular energy in the form of ATP through oxidative phosphorylation (OXPHOS). During this process, four multiprotein complexes located in the inner mitochondrial membrane transfer electrons in a series of redox reactions that creates a proton electrochemical gradient across the membrane. Complex V (ATP synthase or F0F1-ATPase) is a fifth multisubunit complex, which generates ATP using the energy created by the proton electrochemical gradient. ATP synthesis and hydrolysis by complex V is a sophisticated process that depends on the coordinated expression of nuclear and mitochondrial genes and the assembly and function of several subunits as an active complex. As a result of the centrality of mitochondrial energy generation in all vital cellular functions, impairment of this process in the mitochondria is strongly associated with aging and pathology in neurodegenerative disorders, cardiovascular diseases, diabetes, and cancer (Wallace, 2005).

Protein acetylation is emerging as a major posttranslational modification, and it involves reversible acetylation of the ε-amino group of internal lysine residues, which is regulated by lysine acetyltransferases and lysine deacetylases (Kouzarides, 2000; Yang, 2004). In recent years, the class III histone deacetylases, the sirtuins, have emerged as prominent deacetylases (Haigis and Sinclair, 2010; Zhao et al., 2010; Lombard et al., 2011; Newman et al., 2012; Xiong and Guan, 2012). Mammals contain seven sirtuins: SIRT1, SIRT6, and SIRT7 are nuclear; SIRT2 is predominantly cytoplasmic; and SIRT3, SIRT4, and SIRT5 localize to the mitochondria. There are five sirtuins in *Drosophila melanogaster*—Sir2 (CG5216), Sirt2 (CG5085), Sirt4 (CG3187), Sirt6 (CG6284), and Sirt7 (CG11305). BLAST (Basic Local Alignment Search Tool) searches reveal that *Drosophila* Sir2 shares 42% sequence identity with human SIR2, dSirt2 shows 49% identity to SIRT2 and 50% identity to human SIRT3, dSirt4 shares 49% identity with human SIRT4, dSirt6

M. Rahman, N.K. Nirala, and A. Singh contributed equally to this paper.

Correspondence to Usha R. Acharya: usha.acharya@umassmed.edu

Abbreviations used in this paper: BN, blue native; GO, gene ontology; LC, liquid chromatography; OXPHOS, oxidative phosphorylation; ROS, reactive oxygen species; UAS, upstream activation sequence.

The Rockefeller University Press $30.00
J. Cell Biol. Vol. 206 No. 2 289–305
www.jcb.org/cgi/doi/10.1083/jcb.201404118

shows 50% identity to human SIRT6, and dSirt7 shows 46% identity to human SIRT7. dSir2 is the most well characterized among the *Drosophila* sirtuins. It is an essential gene that is expressed during development, and its localization is thought to be both cytoplasmic and nuclear. Sir2 is required for heterochromatic gene silencing and euchromatic repression (Rosenberg and Parkhurst, 2002). Earlier studies have also demonstrated roles for *Drosophila* Sir2 in life span extension and regulation of cell death and survival (Wood et al., 2004; Griswold et al., 2008; Banerjee et al., 2012). Sir2 has also been identified as a negative regulator of fat storage in *Drosophila* larvae (Reis et al., 2010). A neuroprotective role has been suggested for Sirt2 because its loss leads to rescue of photoreceptor death observed in *Drosophila* models of Huntington's disease (Luthi-Carter et al., 2010). Sirtuin activity depends on NAD^+, which suggests that their activity is linked to the energy status of the cell via the NAD^+/NADH ratio (Imai et al., 2000; Houtkooper et al., 2010; Imai and Guarente, 2010).

Global proteomic surveys have shown that mitochondrial proteins are extensively modified by lysine acetylation (Kim et al., 2006; Lombard et al., 2007; Choudhary et al., 2009; Hebert et al., 2013; Rardin et al., 2013). SIRT3 appears to be the major mitochondrial deacetylase. SIRT3-deficient mice exhibit mitochondrial protein hyperacetylation, whereas no significant changes were observed in *SIRT4*$^{-/-}$ and *SIRT5*$^{-/-}$ mitochondria. Despite the increased acetylation of proteins, germline deletion of SIRT3 or deletion of SIRT3 in a muscle- or liver-specific manner does not result in overt metabolic phenotypes (Lombard et al., 2007; Fernandez-Marcos et al., 2012). However, under conditions of stress such as fasting or caloric restriction, SIRT3 has been shown to regulate fatty acid oxidation by activating long chain acyl-CoA (coenzyme A) dehydrogenase, ketone body production through 3-hydroxy-3-methylglutaryl CoA synthase 2, in mitigating reactive oxygen species (ROS) damage by deacetylating superoxide dismutase, and protecting mice from age-related hearing loss through activation of isocitrate dehydrogenase (Hirschey et al., 2010; Qiu et al., 2010; Shimazu et al., 2010; Someya et al., 2010; Tao et al., 2010; Chen et al., 2011). A role for SIRT3 has been implicated in regulating OXPHOS because germline *Sirt3*$^{-/-}$ mice show a decrease in ATP levels in different organs (Ahn et al., 2008; Cimen et al., 2010; Finley et al., 2011b; Shinmura et al., 2011; Wu et al., 2013). However, muscle- or liver-specific deletion of SIRT3 did not result in changes in ATP levels, suggesting that SIRT3 deletion in a tissue-specific manner does not affect cellular energy levels (Fernandez-Marcos et al., 2012). In this study, we have used *Drosophila* as a model and performed mass spectrometric analyses on wild-type and *dsirt2* mutant flies to identify the *Drosophila* mitochondrial and dSirt2-regulated acetylome. Our proteomic experiments show *Drosophila* Sirt2 is an important regulator of mitochondrial function and is the functional homologue of mammalian SIRT3. These experiments also provide a comprehensive view of the impact of acetylation on OXPHOS and its regulation by dSirt2. We demonstrate that ATP synthase β, the catalytic subunit of complex V, is an acetylated protein, and it is a substrate of *Drosophila* Sirt2 and human SIRT3.

In this study, we also reveal a novel connection between NAD metabolism, sirtuins, and the sphingolipid ceramide. Sphingolipids are an essential class of lipids that are building blocks for membranes and serve as transducers in signaling cascades that regulate cell growth and death (Hannun and Obeid, 2008). Ceramide, a central intermediate in sphingolipid metabolism, mediates many stress responses, and recent literature highlights that perturbations in ceramide levels can affect glucose and fat metabolism (Bikman and Summers, 2011). How ceramide and other sphingolipids affect cellular metabolism, what metabolic pathways they impinge on, and identification of the ensuing functional consequences are only beginning to be explored. We show that *Drosophila* mutants of sphingolipid metabolism, particularly, ceramide kinase mutants (*dcerk*^{1}), have increased levels of ceramide and decreased levels of NAD^+. This results in reduced dSirt2 activity in *dcerk*^{1} mutants, leading to acetylation of several subunits of complex V, including ATP synthase β and reduced complex V activity. These experiments reveal a novel axis involving ceramide, NAD, and sirtuins.

Results

Ceramide increase affects NAD^+ level and sirtuin activity

We performed metabolomic profiling on sphingolipid mutants that accumulate ceramide to gain insight into metabolic pathways that could be altered in these mutants. Our earlier study combined metabolomic profiling with genetic and biochemical approaches and demonstrated that *dcerk*^{1} mutants show an increased reliance on glycolysis, which leads to an increase in lactate to compensate for the decreased production of ATP through OXPHOS (Nirala et al., 2013). The increase in glycolytic flux is also observed in a mammalian model of ceramide increase, mice heterozygous for the ceramide transfer protein (Wang et al., 2009; Nirala et al., 2013). In addition to changes in glycolytic intermediates, metabolomic profiling revealed that *dcerk*^{1} mutants have a significantly decreased level of NAD^+ compared with that in w^{1118} (control) flies (Fig. 1 A). The NAD^+ level is controlled by balancing synthesis, salvage, and consumption pathways (Fig. 1 B). Like in mammals, NAD^+ can be synthesized in *Drosophila* from the salvage pathway from nicotinic acid, nicotinamide, and nicotinamide riboside (nicotinamide mononucleotide) and by the de novo pathway from tryptophan (Zhai et al., 2006; Campesan et al., 2011). We used mass spectrometry (MS) to measure the levels of intermediates in these pathways and related metabolites. The levels of key intermediates, such as nicotinamide riboside in the salvage pathway and hydroxykynurenine in the de novo pathway, of NAD^+ synthesis in *dcerk*^{1} are increased compared with those in controls, suggesting that synthesis pathways do not appear to be compromised (Fig. 1 C). We then tested whether the NAD^+ level is altered in the ceramidase mutant (*cdase*^{1}), another mutant of the sphingolipid pathway that accumulates ceramide (Acharya et al., 2008). The NAD^+ level is also decreased in *cdase*^{1} (Fig. S1). Estimation of intermediates of the salvage and de novo pathways of NAD^+ synthesis in *cdase*^{1} reveals a fivefold increase in 3-hydroxy kynurenine, which suggests a compensatory increase

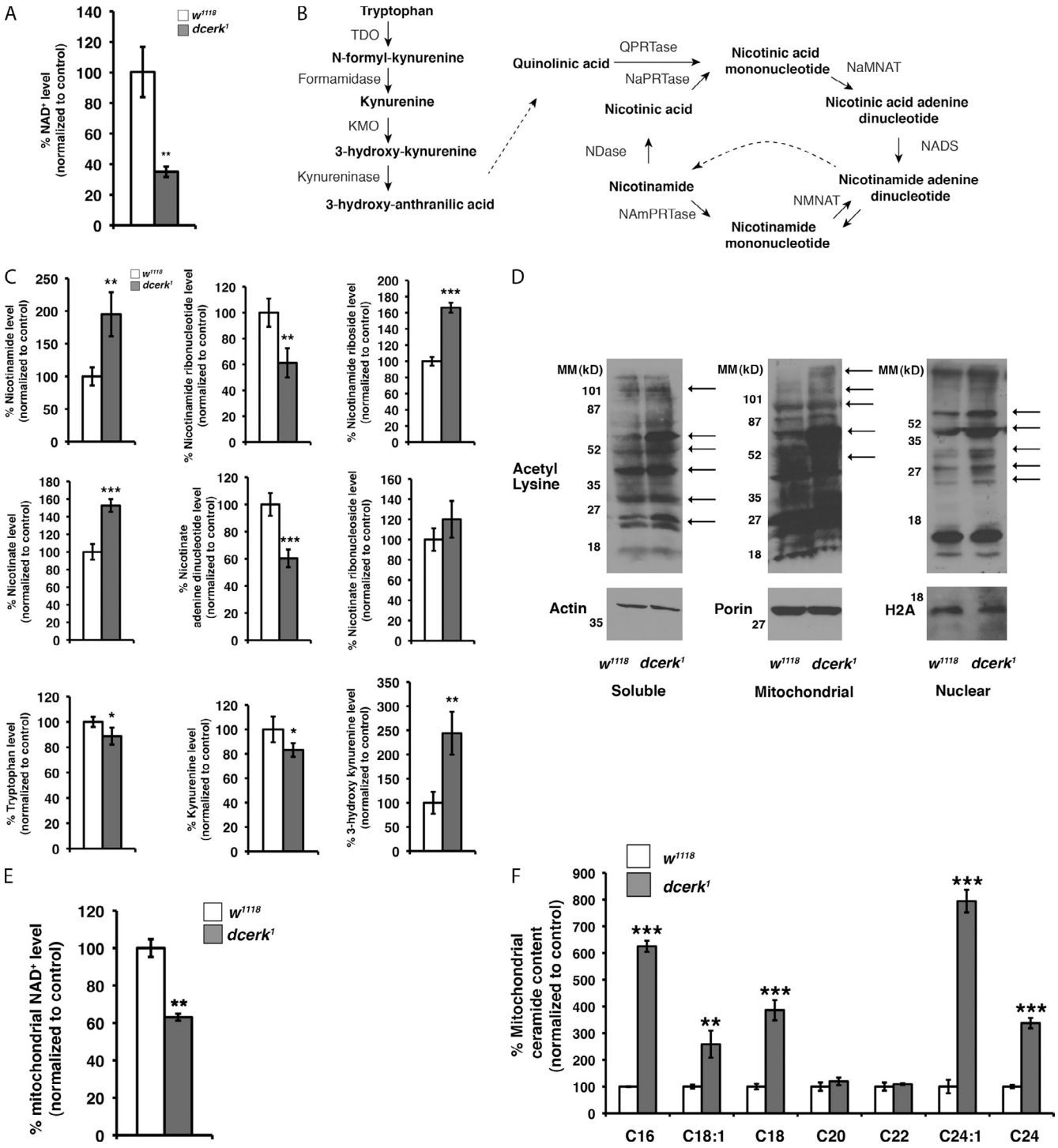

Figure 1. **Increase in ceramide levels results in depletion of NAD⁺ and decrease in sirtuin activity leading to hyperacetylation of proteins in different cellular compartments.** (A) *dcerk*^{1} fly extracts show 65% reduction in NAD⁺ level compared with w^{1118} control. *n* = 3. (B) NAD synthesis and salvage pathways. TDO, tryptophan-2,3-dioxygenase; KMO, kynurenine 3-monooxygenase; QPRTase, quinolinate phosphoribosyltransferase; NaMNAT, nicotinic acid mononucleotide adenyltransferase; NADS, NAD synthetase; NMNAT, nicotinamide mononucleotide adenyltransferase; NAmPRTase, nicotinamide phosphoribosyl transferase; NDase, nicotinamidase; NaPRTase, nicotinic acid phosphoribosyltransferase. (C) Mass spectrometric measurements of metabolites in the salvage and the de novo pathways for synthesis of NAD⁺. *n* = 3. (D) Soluble, mitochondrial, and nuclear extracts were prepared from w^{1118} and *dcerk*^{1} mutant flies and separated by PAGE. Protein acetylation was monitored by Western blotting using an anti–acetyl-Lys antibody. The individual blots were probed with antibodies to actin, porin, and H2A as loading controls. *dcerk*^{1} mutants show protein hyperacetylation in the different cellular compartments. Arrows indicate proteins that are hyperacetylated in *dcerk*^{1} compared with w^{1118}. MM, molecular mass. (E) Mitochondrial NAD⁺ levels are decreased in *dcerk*^{1} compared with control. (F) d14 long chain base ceramides with different fatty acids were estimated by MS in sphingolipid-enriched fractions prepared from w^{1118} and *dcerk*^{1} mitochondria. C denotes the carbon chain length of fatty acids in the different ceramides. The amount of ceramide is normalized to total carbon content, and the level in w^{1118} is taken as 100%. Many ceramides show significant increase in the mutant mitochondria compared with w^{1118}. *n* = 3. Error bars represent SDs. *, P ≤ 0.05–0.01; **, P ≤ 0.01–0.001; ***, P ≤ 0.001–0.0001 in Student's *t* test.

A

Gene	Proteins identified by mass spectrometry in *dcerk*^{1}	Acetylation status
Complex II	**Succinate Dehydrogenase**	
CG17246	Succinate Dehydrogenase A	acetylated
CG3283	Succinate Dehydrogenase B	
Complex III	**Ubiquinol-Cytochrome C Reductase**	
CG3731	Core Protein 1	acetylated
CG4169	Core Protein 2	acetylated
CG4769	Cytochrome C1	acetylated
CG7361	Iron-sulfur Subunit	
CG3560	UCR6, 14kD	
CG8764	UCRX, 7.2kD	
CG7580	Ubiquinone Binding Protein	
CG41623	UCRH, 11kD	
Complex IV	**Cytochrome C Oxidase**	
CG34067	Subunit I	
CG34069	Subunit II	
CG10664	Subunit IV	
CG14724	Subunit Va	acetylated
CG17280	Subunit VIa	
CG14235	Subunit VIb	
CG14028	Subunit VIc	
Complex V	**ATP Synthase**	
CG3612	ATP Synthase α	acetylated
CG11154	ATP Synthase β	acetylated
CG7160	ATP Synthase γ	acetylated
CG2968	ATP Synthase δ	
CG9032	ATP Synthase ε	
CG4307	ATP Synthase O	acetylated
CG8189	ATP Synthase b	acetylated
CG6030	ATP Synthase d	
CG3321	ATP Synthase e	
CG4692	ATP Synthase f	
CG6105	ATP Synthase g	acetylated
CG4412	ATPase Coupling Factor 6	

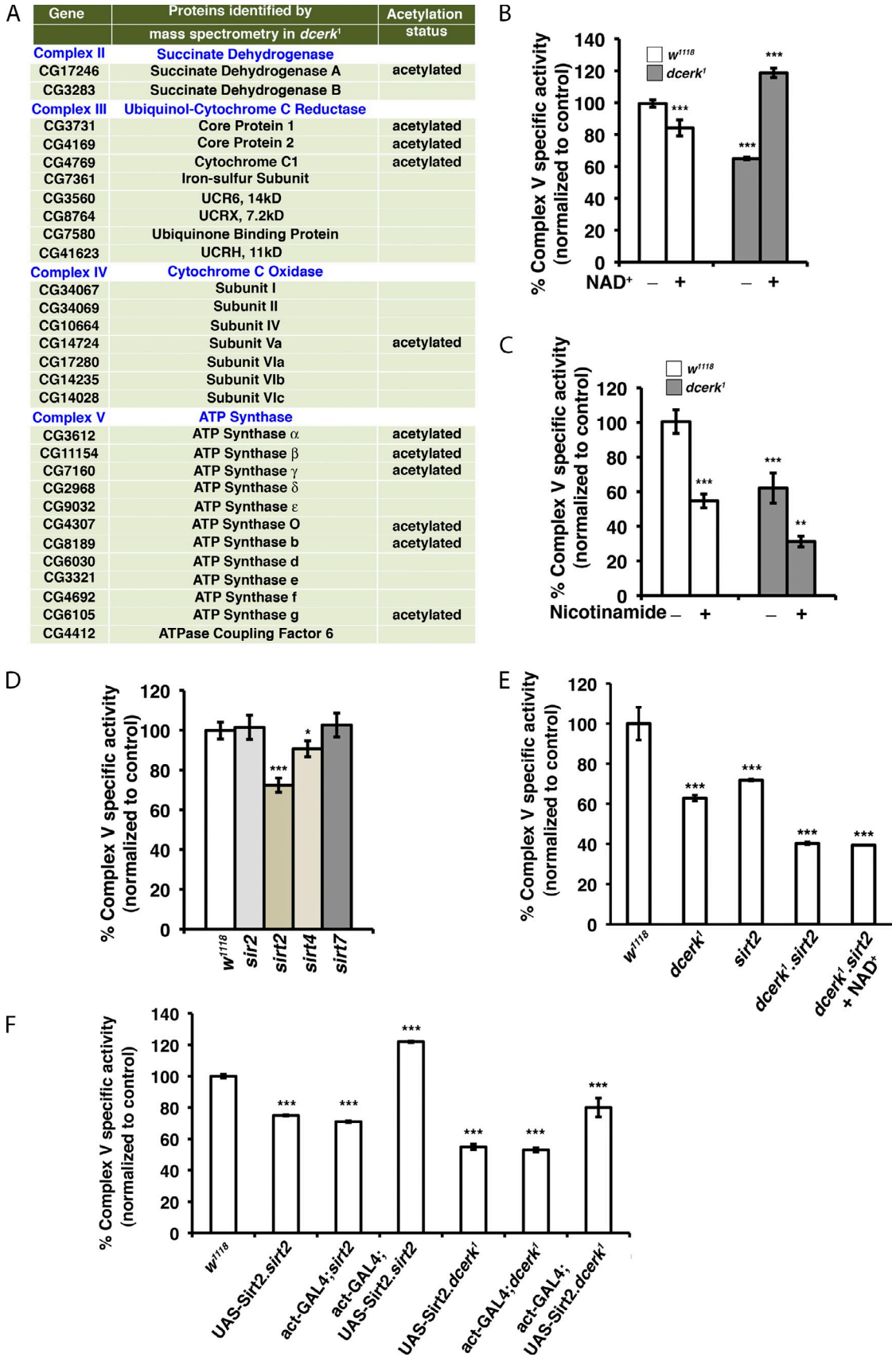

Figure 2. ***dcerk*^{1} mutants show acetylation of many OXPHOS subunits and decrease in complex V activity, which is rescued by supplementing NAD$^+$ and inhibited by nicotinamide.** dSirt2 regulates complex V activity in *dcerk*^{1} mutants. (A) BN-PAGE–separated bands from *dcerk*^{1} were digested with trypsin and subjected to LC-MS/MS to identify the different subunits of the complexes and the subunits that are acetylated. (B) *dcerk*^{1} mitochondria show a 40% reduction in complex V activity. Supplementing with NAD$^+$ restores complex V activity in *dcerk*^{1}. Complex V activity was normalized to the activity of

in tryptophan metabolism in an attempt to maintain NAD^+ levels. These results suggest a connection between ceramide and NAD metabolism.

One of the main NAD^+-consuming pathways involves sirtuins because they are NAD^+-dependent enzymes, and the availability of NAD^+ is an important mechanism that regulates their activity (Imai et al., 2000). *dcerk*^{1} had greater decreases in NAD^+ levels compared with those in *cdase*^{1}; therefore, we investigated this mutant in more detail. As a readout for sirtuin activity in *dcerk*^{1}, we compared the acetylation status of proteins in extracts prepared from different cellular compartments by western analysis using a pan–acetyl-Lys antibody. Fig. 1 D shows that protein acetylation is increased in soluble, nuclear, and mitochondrial extracts of *dcerk*^{1} compared with those in control extracts, suggesting a likely decrease in sirtuin deacetylase activity in *dcerk*^{1}. We decided to focus on the mitochondrial compartment because *dcerk*^{1} exhibits phenotypes associated with mitochondrial dysfunction. These include decreased OXPHOS and decreased mitochondrial ATP level (Nirala et al., 2013). To test whether NAD^+ level is altered in the mitochondria, we estimated its level in mitochondria isolated from w^{1118} and *dcerk*^{1} flies. Indeed, the mitochondrial NAD^+ level is decreased in *dcerk*^{1} (Fig. 1 E). We estimated different ceramides by MS in purified mitochondria isolated from *dcerk*^{1} and w^{1118} to test whether ceramide levels are increased in mutant mitochondria (Dasgupta et al., 2009). Many ceramides show significantly increased levels in *dcerk*^{1} mitochondria compared with those in the control (Fig. 1 F). The experiments described in the following sections probe the correlation between *dcerk*^{1}, sirtuin function, the acetylation of mitochondrial proteins, and its impact on mitochondrial function.

Several OXPHOS proteins including those of complex V are acetylated in *dcerk*^{1} mutants

To investigate the increase in mitochondrial Lys acetylation observed in *dcerk*^{1}, we decided to focus on OXPHOS because it plays a central role in mitochondrial function. We prepared mitochondria from control and *dcerk*^{1} flies and resolved individual OXPHOS complexes by blue native (BN) PAGE (Fig. S2 A). BN-PAGE allows for separation of complexes in their native state, which enables assessment of both the amount and activity of complexes (Wittig et al., 2006). We confirmed the identity of each complex by in-gel activity staining. As seen from the Coomassie-stained gel, the amount of complexes is not different in control and mutant mitochondria, whereas activity staining suggested that activities of complexes II, III, IV, and V were reduced in *dcerk*^{1} mutant flies. Each band (other than complex I, which could not be isolated in sufficient amounts to identify a majority of its 50 subunits) was subjected to proteolytic digestion and analyzed by liquid chromatography (LC)–MS/MS. The proteins identified in each complex in *dcerk*^{1} and those that are acetylated are shown in Fig. 2 A. Acetylated proteins were identified in each of the four complexes, suggesting that it could be a prevalent modification among OXPHOS proteins. Of the four complexes, we chose complex V for detailed analyses because it showed the largest number of acetylated proteins and because it directly controls ATP synthesis and hydrolysis, thereby strongly influencing cellular ATP levels.

Drosophila sirt2 mutants regulate complex V activity

Complex V catalyzes both ATP synthesis and ATP hydrolysis coupled with transmembrane proton translocation in mitochondria (Boyer, 1997). The enzyme has two moieties—the water-soluble F1 portion, which contains the catalytic sites for ATP generation and hydrolysis, and the membrane-integrated F0 portion, which mediates proton translocation (Abrahams et al., 1994; Noji et al., 1997). The enzymatic complex consists of a catalytic headpiece ($\alpha_3\beta_3$) that contains the three catalytic sites for ATP synthesis (one in each β subunit), a proton channel (ac_8) and two stalks, the central rotor (γ, δ, and ε), and the peripheral stator (bdF_6OSCP).

dcerk^1 mutants display a 40% decrease in complex V ATPase activity compared with that of control (Fig. 2, B and C). Because this decrease in activity was accompanied by decreased NAD^+ and increased acetylation of complex V subunits, we tested whether we could rescue complex V activity in *dcerk*^{1} by supplementing with NAD^+. We raised *dcerk*^{1} flies for a short period of time in food supplemented with NAD^+ and measured complex V activity. Supplementing with NAD^+ rescues the ATPase activity in *dcerk*^{1} (Fig. 2 B). Supplementing high concentrations of nicotinamide, an inhibitor of sirtuin, further decreases complex V activity in the mutants (Fig. 2 C). We estimated NAD^+ and nicotinamide levels in wild-type flies supplemented with a high concentration of nicotinamide in the food. Although there is a very modest increase in NAD^+ level, there is a substantial increase in nicotinamide in the fed flies as a result of feeding pharmacological amount of nicotinamide in these flies (Fig. S2 B). These results show that complex V activity can be modulated by activation of a sirtuin with NAD^+ or inhibition of a sirtuin with nicotinamide.

To test whether any of the five *Drosophila* sirtuins could regulate complex V, we measured ATPase activity of the complex in mitochondria prepared from *sir2*-, *sirt2*-, *sirt4*-, and

citrate synthase, a mitochondrial marker. The ATPase activity of untreated w^{1118} was taken as 100%. (C) Nicotinamide treatment further inhibits complex V activity in *dcerk*^{1}. The ATPase activity of untreated w^{1118} was taken as 100%. $n = 3$. (D) Mitochondria were isolated from different sirtuin-null mutants, and complex V activity was measured. Complex V activity was normalized to the activity of citrate synthase. The ATPase activity of w^{1118} was taken as 100%. *dsirt2* mutants show 30% reduction in activity. $n = 3$. (E) Mitochondria were isolated from w^{1118}, *dcerk*^{1}, *dsirt2*, *dcerk*^{1}.*dsirt2*, and *dcerk*^{1}.*dsirt2* raised on food supplemented with NAD^+, and complex V activity was measured. The ATPase activity of w^{1118} was taken as 100%. *dcerk*^{1}.*dsirt2* mutants show a further reduction in complex V activity compared with the single mutants. Supplementing with NAD^+ does not alter this activity. $n = 3$. (F) The wild-type Sirt2 transgene was ubiquitously overexpressed using the actin-GAL4 driver in *dsirt2* and *dcerk*^{1} mutants. The UAS-Sirt2 transgenic and GAL4 driver in each genetic background were additional controls. Mitochondria were prepared, and complex V activity was measured. The activity of w^{1118} was taken as 100%. Overexpression of the Sirt2 transgene significantly rescues complex V activity in the *dsirt2* mutant and partially in the *dcerk*^{1} mutant. Error bars represent SDs. *, $P \leq 0.05$–0.01; ** $P \leq 0.01$–0.001; *** $P \leq 0.001$–0.0001 in Student's *t* test.

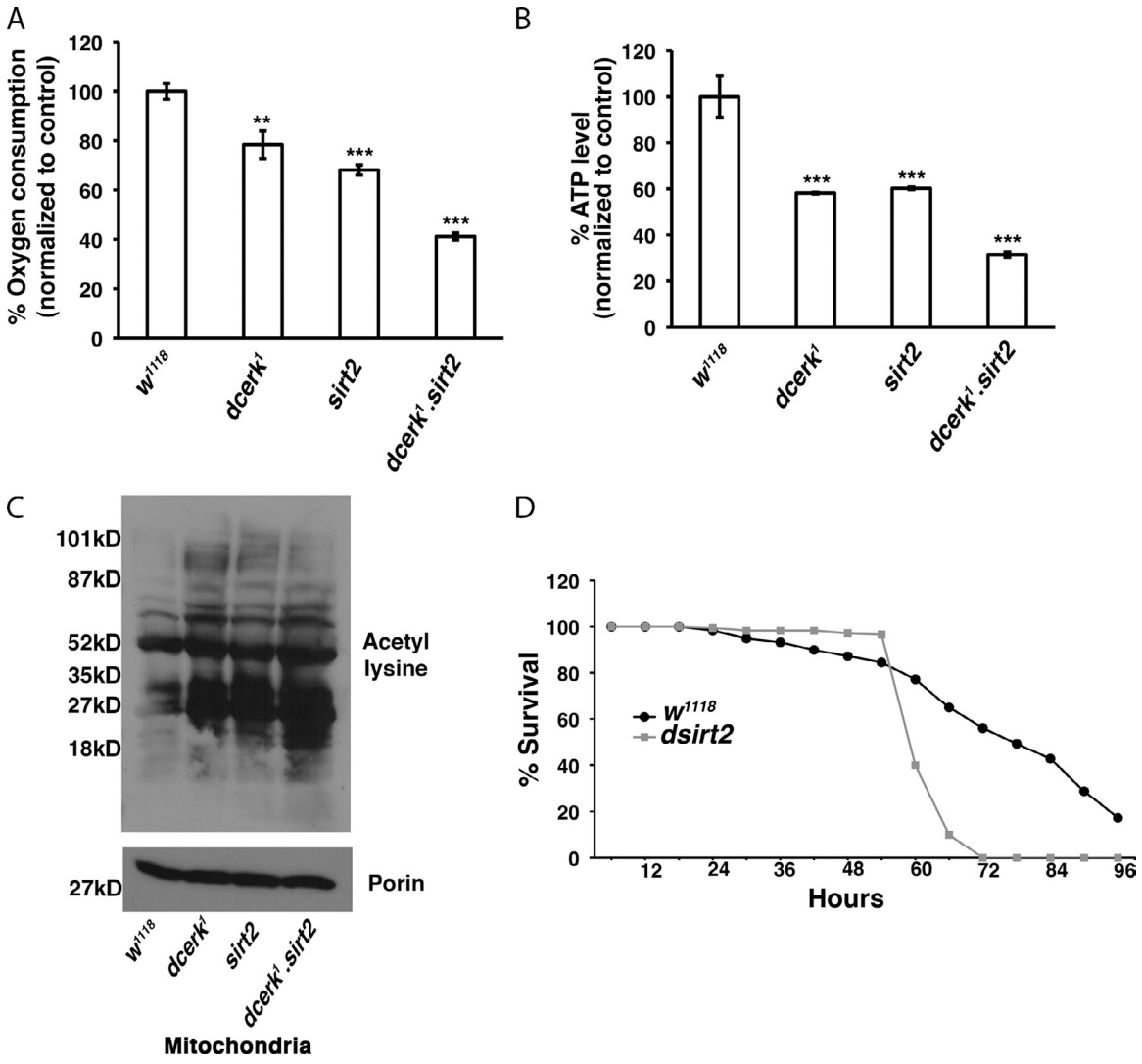

Figure 3. **Loss of sirt2 further reduces oxygen consumption and ATP levels and further increases mitochondrial protein acetylation in *dcerk*^{1} mutants.** (A) Oxygen consumption was measured in freshly isolated mitochondria after addition of ADP (state 3 respiration). It is decreased in both *dcerk*^{1} and *dsirt2* mutant mitochondria compared with w^{1118}. The double mutants show a further decrease in oxygen consumption. (B) ATP level is measured in w^{1118}, *dcerk*^{1}, *sirt2*, and *dcerk*^{1}.*dsirt2* fly mitochondria. The amount of ATP is calculated per milligram of mitochondrial protein and normalized to w^{1118}. The relative level of ATP in individual *dcerk*^{1} and *sirt2* is 60%, and the double mutant is 35% of w^{1118}. (A and B) $n = 3$; error bars represent SDs. **, $P \leq 0.01$–0.001; ***, $P \leq 0.001$–0.0001 in Student's *t* test. (C) Mitochondrial extracts were prepared from w^{1118}, *dcerk*^{1}, *sirt2*, and *dcerk*^{1}.*dsirt2* flies and separated by PAGE followed by Western blotting using an anti–acetyl-Lys antibody. The blot was probed with an antibody to porin as a loading control. *dcerk*^{1}.*dsirt2* double mutants show a further increase in protein acetylation compared with individual mutants. (D) Wild type and *dsirt2* are subjected to starvation and the number of surviving flies is recorded at 6-h intervals. 200 flies divided into 10 groups for each genotype are used in one experiment. The representative graph shows the percentage of survival for each time interval.

sirt7-null mutants (Xie and Golic, 2004). Because Sirt6-null mutants are not available, Sirt6 knockdown flies were used, and this did not result in a significant reduction of complex V activity (unpublished data). Fig. 2 D shows that *sirt2* mutant mitochondria display ∼30% reduction in ATPase activity compared with control. We then generated *dcerk*^{1}.*dsirt2* double mutants and assessed complex V activity. As seen in Fig. 2 E, there is a further reduction in complex V activity of *dcerk*^{1} in the absence of sirt2. Furthermore, feeding NAD^+ does not rescue complex V activity of *dcerk*^{1} mutants in the absence of sirt2 (Fig. 2 E). In addition, the double mutants are semilethal, whereas individual mutants are viable, supporting a genetic interaction between these two mutants. Ubiquitous overexpression of a wild-type copy of the *Sirt2* transgene (using the actin-Gal4 driver) in the *sirt2* mutant results in a significant increase in complex V activity (Fig. 2 F). Overexpression of wild-type *Sirt2* in the *dcerk*^{1} mutant results in partial rescue. Overexpressed *Sirt2* could compete for the limited NAD^+ in *dcerk*^{1} and result in better deacetylation of its substrates, including complex V, thereby leading to partial rescue (Fig. 2 F).

We also measured the ATP synthase activity in *dcerk*^{1} and *dsirt2* single and *dcerk*^{1}.*dsirt2* double mutant flies. In intact mitochondria, the amount of oxygen consumption reflects the amount of ATP synthesis, and inhibition of ATP synthase or other OXPHOS complexes can cause a decrease in oxygen consumption. We measured state 3 respiration (in the presence of added ADP) in freshly isolated mitochondria from the different flies. The *dcerk*^{1} and *dsirt2* mitochondria displayed decreased

oxygen consumption and decreased ADP responsiveness compared with that in control, suggesting that the rate of ATP synthesis via OXPHOS was lower in the mutants compared with that in the control (Fig. 3 A). Absence of sirt2 further decreases the rate in *dcerk*^{1} as observed in *dcerk*^{1}.*dsirt2* double mutant flies (Fig. 3 A). We measured the ATP level in mitochondria isolated from *w*^{1118}, *dcerk*^{1}, and *dsirt2* single mutants and *dcerk*^{1}.*dsirt2* double mutants. Indeed, *dcerk*^{1} and *dsirt2* show a 40% reduction in ATP levels compared with *w*^{1118}, whereas there is a further decrease in the double mutants (Fig. 3 B). These results suggest that *Drosophila* Sirt2 is a primary regulator of complex V activity in the *dcerk*^{1} mutant. Because absence of Sirt2 exacerbates complex V activity and ATP level of *dcerk*^{1}, we also tested whether loss of Sirt2 would further increase the acetylation of mitochondrial proteins observed in *dcerk*^{1}. Indeed, mitochondrial proteins from *dcerk*^{1}.*dsirt2* double mutants show increased acetylation compared with the single mutants (Fig. 3 C). We then tested how *dsirt2* mutant flies respond to conditions such as starvation stress, which increase ATP demand. *dsirt2* mutants succumb to starvation stress more rapidly than wild-type flies (Fig. 3 D). The decreased ATP synthetic capacity in the mutants likely exacerbates the starvation survival response. *dcerk*^{1} mutants, however, do not show increased sensitivity to starvation because of AKT/FOXO-mediated up-regulation of novel triglyceride lipases (Nirala et al., 2013). A further indication of mitochondrial dysfunction in the *dsirt2* mutant is the increased ROS level (Fig. S3).

Drosophila mitochondrial protein acetylome and dSirt2-regulated acetylome

To begin to understand how dSirt2 influences mitochondrial protein acetylation, we characterized the mitochondrial acetylome in wild-type and *dsirt2* flies by quantitative MS. Previously, one proteome-wide mapping of the *Drosophila* acetylome has been performed from embryonically derived SL2 tissue-culture cells (Weinert et al., 2011). However, no proteomic investigations of either the total or mitochondrial acetylome have been performed in flies. The strategy we used for identification of the *Drosophila* mitochondrial acetylome and the dSirt2-regulated acetylome is outlined in Fig. S4. We identified 1,178 unique acetyl-Lys sites in 530 proteins. Of these, 652 unique acetyl-Lys sites in 214 proteins were identified as mitochondrial using FlyBase and MitoDrome, a database of *Drosophila* nuclear genes coding for mitochondrial proteins (Table S1; Sardiello et al., 2003). The identification of a large set of acetylated proteins enabled a systematic analysis of these proteins.

Pathway analysis of the *Drosophila* mitochondrial protein acetylome reveals widespread acetylation of OXPHOS proteins and other metabolic pathways

We performed functional annotation to determine the gene ontology (GO) terms associated with the acetylated proteins in wild-type control flies. The cellular component ontology, which describes protein location at the substructural level, shows a significant enrichment of mitochondrial-associated terms (Fig. 4 A). Analysis of the distribution of the number of acetyl-Lys sites detected per mitochondrial protein shows that 43% of the proteins have one identifiable site, whereas the remainder have two or more sites, which suggests multiple points of regulation for a given protein (Fig. 4 B).

To gain insight into the biological functions of the acetylated proteins, we performed a pathway enrichment analysis of the mitochondrial acetylated proteins. Fig. 4 C shows that there is significant enrichment of proteins involved in the respiratory electron transport chain and enzymes involved in pyruvate metabolism, TCA cycle, and amino acid metabolism. Other pathways identified include β-oxidation of fatty acids, branched-chain amino acid catabolism, ketone body metabolism, and antioxidant metabolism. In addition, our study identifies acetylated proteins in Lys catabolism (lysine ketoglutarate reductase), β-oxidation of pristanoyl CoA (pristanoyl CoA oxidase), and ω fatty acid metabolism. To visualize probable consensus patterns around the acetyl-Lys sites, we compared the amino acid sequences of all acetylated sites using iceLogo (Colaert, et al., 2009). A preference for Leu or Tyr is observed at the +1 position, and a preference for Asp is observed at the −1 and −3 positions, whereas positively charged residues are excluded at these positions (Fig. 4 D).

Analysis of the dSirt2-regulated acetylome identifies substrates in OXPHOS and metabolic pathways

A comparison of the wild-type *Drosophila* mitochondrial acetylome to that of *dsirt2* mitochondria identifies that 204 acetylation sites in 116 proteins increased >1.5-fold in the mutant (Table S2). The GO cellular component analysis showed a significant enrichment of mitochondrial terms (Fig. 4 E). Pathways enriched in the *dsirt2* mutant included TCA cycle, amino acid metabolism, and electron transport chain (Fig. 4 F). Previously validated substrates of mouse Sirt3, such as succinate dehydrogenase A, isocitrate dehydrogenase 2, and long chain acyl-CoA dehydrogenase, are identified in our study. These results suggest that *Drosophila* Sirt2 could serve as the functional homologue of mammalian SIRT3. In addition, mammalian SIRT3 shows highest homology (50% identity and 64% similarity) to *Drosophila* Sirt2.

Analyses of flanking sequence preferences in acetylated proteins that are increased in *dsirt2* suggest a preference for Arg at the +1 site and exclusion of positive charge at the −1 position (Fig. 4 G). The molecular function and biological process components of GO reveal significant enrichment of different complexes of the electron transport chain, with complex I being most significant followed by complex V in the wild-type mitochondrial acetylome (Fig. 5 A). The distribution of acetyl-Lys sites among the electron transport chain complexes suggests that 30% of the acetylated subunits have one Lys site, whereas 70% have more than one site (Fig. 5 B). GO shows that both complex I and complex V feature prominently in the Sirt2 mutant acetylome (Fig. 5 C). Fig. 5 D shows a list of complex V subunits with site-specific acetyl-Lys identified earlier in *dcerk*^{1} and those that change 1.5-fold or more in *dsirt2*. To understand how complex V activity could be influenced by reversible acetylation, we focused on ATP synthase β, as it is the catalytic subunit of the complex. We performed subsequent experiments in mammalian

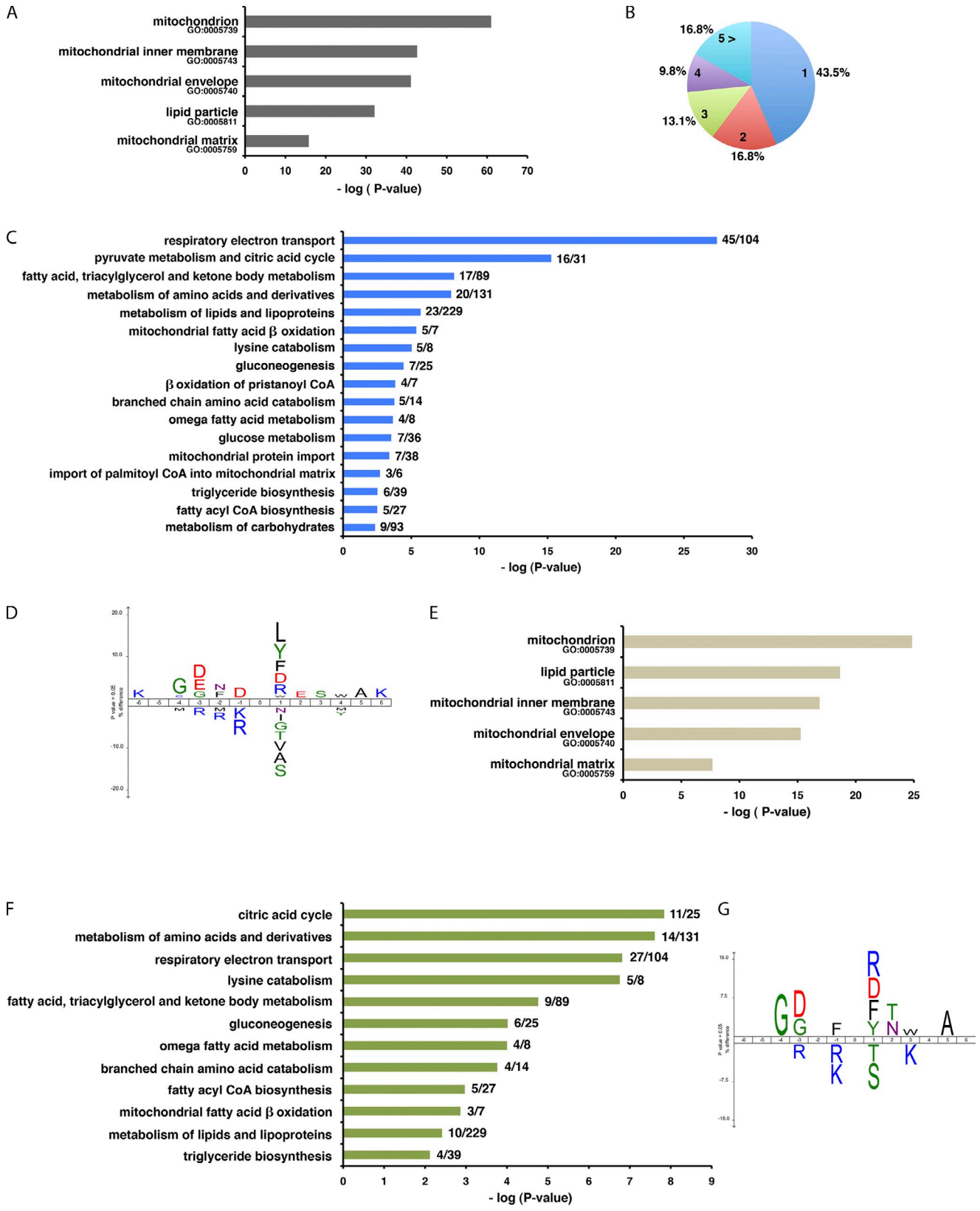

Figure 4. **Analyses of the *Drosophila* mitochondrial acetylome and dSirt2 acetylome reveal extensive acetylation of proteins engaged in OXPHOS and metabolic pathways involved in energy production.** (A) GO analysis (cellular component) of the acetylome shows significant enrichment of mitochondria-related terms. (B) Distribution of acetyl-Lys sites identified per protein in the mitochondrial acetylome. (C) Pathway analysis of the mitochondrial acetylome with the number of proteins identified per pathway indicated. (D) Consensus sequence logo plot for acetylation sites, ±6 amino acids from all acetyl-Lys identified in the mitochondrial acetylome. (E) GO analysis (cellular component) of the acetylated proteins that increase in the *dsirt2* mutant. (F) Pathway analysis of the acetylated proteins that increase in *dsirt2* with the number of proteins identified per pathway indicated. (G) Consensus sequence logo plot for acetylation sites, ±6 amino acids from all acetyl-Lys identified in proteins that increase in *dsirt2*.

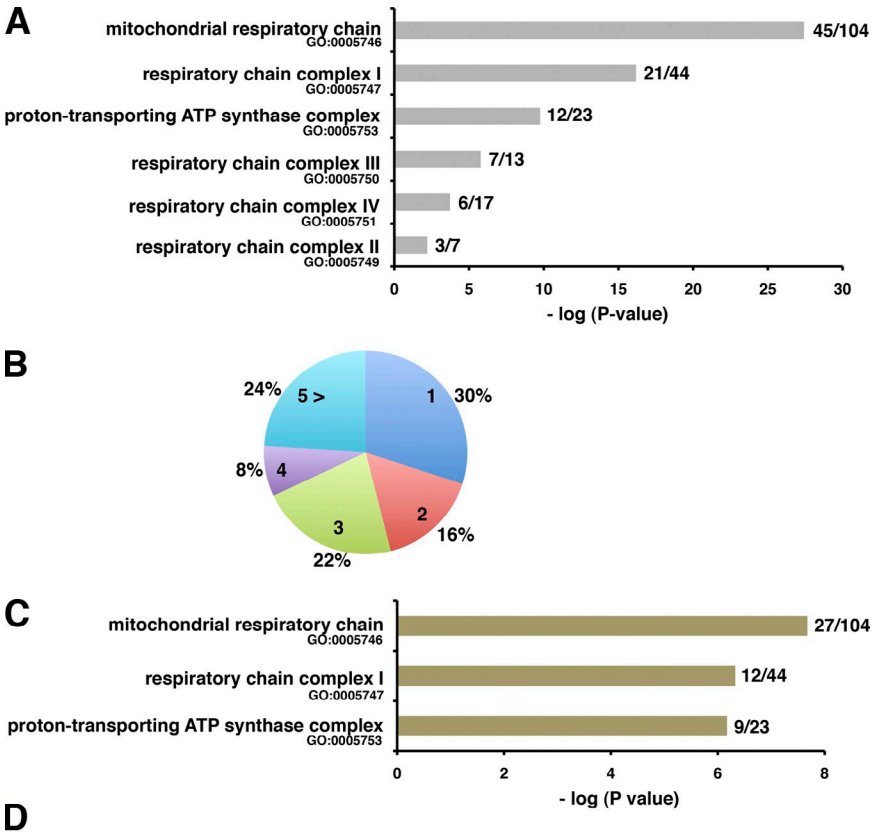

D

Gene	Protein	*dcerk*[1] (Lys)	*sirt2* (Lys)	Human (Lys)
CG3612	ATP synthase α	64	64	
		160	160	161*
		260	260	261*
		515	515	
		166		167*
		240		241*
		433		434*
			304	305
			423	
			502	503
			527	
			538	539*
			540	541
			545	
CG11154	ATP synthase β	236	236	259*
		457	457	480*
		189		212*
		328		351*
		428		451
CG7610	ATP synthase γ	167	167	
			88	88*
CG2968	ATP synthase δ	none	137	
CG9032	ATP synthase ε	none	43	44

Gene	Protein	*dcerk*[1] (Lys)	*sirt2* (Lys)	Human (Lys)
CG4307	ATP synthase O (OSCP)	46	46	51
			151	
CG8189	ATP synthase b	126	126	
CG6030	ATP synthase d	none	78	78*
			167	
CG3321	ATP synthase e	76	76	
			80	
CG4692	ATP synthase f	none	none	
CG6105	ATP synthase g	31	31	35
CG4412	ATPase coupling factor 6		87	

Figure 5. **Identification of complex V subunits with the Lys residues that are acetylated in *dcerk*[1] and *dsirt2* mutants.** (A) GO analysis (biological process component) of the *Drosophila* mitochondrial acetylome shows significant enrichment of OXPHOS complexes, particularly, complex I and complex V. The numbers indicate the number of acetylated subunits out of the total number of OXPHOS subunits in each complex. (B) Distribution of acetyl-Lys sites identified in each acetylated protein of the OXPHOS complexes shows 70% of the proteins have more than one site of acetylation. (C) GO analysis (biological process component) of the acetylated proteins that increase in *dsirt2* features OXPHOS complex I and complex V prominently. The numbers indicate the number of acetylated subunits out of the total number of OXPHOS subunits in each complex in the *dsirt2* mutant. (D) Mass spectrometric identification of the Lys residues that are acetylated in *dcerk*[1] and *dsirt2* (1.5-fold or more) in different subunits of complex V. For Lys residues that are conserved, the corresponding human Lys is shown. Asterisks denote Lys residues that have been identified as acetylated in other proteomic surveys. The blue numbers indicate modified Lys residues identified both in *dcerk*[1] and *dsirt2* mutants.

cells to validate and extend our findings in a mammalian system. The mammalian experiments also benefited from the availability of reagents and tools that are lacking in *Drosophila*.

Human ATP synthase β is an acetylated protein, and SIRT3 regulates its deacetylation and complex V activity

We evaluated whether mammalian ATP synthase β is an acetylated protein. An expression vector encoding DDK-tagged human ATP synthase β or vector alone was transfected into HEK293T cells. After immunoprecipitation with the DDK tag antibody, acetylation level was determined by Western blotting with the acetyl-Lys antibody. ATP synthase β is clearly an acetylated protein (Fig. 6 A). Based on our results from the experiments in *Drosophila* described in the previous sections, we decided to test whether human SIRT3 can modulate the reversible acetylation of ATP synthase β. Knockdown of endogenous SIRT3 by siRNA increased the acetylation of ATP synthase

β (Fig. 6 B). Conversely, overexpression of SIRT3 leads to increased deacetylation of ATP synthase β (Fig. 6 C). To ascertain whether ATP synthase β is a specific target of SIRT3, we knocked down or overexpressed two other mitochondrial sirtuins—SIRT4 and SIRT5. Knockdown of endogenous SIRT4 or SIRT5 by siRNA does not affect acetylation status of ATP synthase β (Fig. 6, D and F). Overexpression of SIRT4 and SIRT5 also does not affect acetylation of ATP synthase β (Fig. 6, E and G). Additionally, knockdown or overexpression of a nuclear sirtuin, SIRT1, also does not impact acetylation of ATP synthase β (Fig. 6, H and I). To determine whether the acetylation state of ATP synthase β altered complex V activity, we measured complex V activity in mitochondria prepared from cells treated with SIRT3 siRNA and scrambled siRNA. Knockdown of SIRT3 results in ∼40% decrease in complex V activity (Fig. 6 J). We tested whether SIRT3 could directly interact with ATP synthase β. We immunoprecipitated endogenous ATP synthase β from HEK293T cells overexpressing SIRT3 and found that SIRT3 could coimmunoprecipitate with ATP synthase β (Fig. 6 K). These results collectively suggest that mammalian SIRT3, like *Drosophila* Sirt2, can influence complex V activity by regulating the acetylation status of ATP synthase β.

Conserved Lys residues in ATP synthase β regulate complex V activity

We identified which Lys residues on ATP synthase β were important for regulating complex V activity. MS analysis of mitochondrial proteins shows that ATP synthase β is hyperacetylated at Lys 236 and Lys 457 in the absence of *Drosophila* Sirt2 (in *dsirt2*). Both these Lys residues were also identified in ATP synthase β in *dcerk*[1]. The equivalent residues in human ATP synthase β are Lys 259 and Lys 480. Before assessing the functional significance of these site-specific Lys residues, we down-regulated endogenous ATP synthase β level in HEK293T cells by siRNA to minimize any contribution from the endogenous protein. We generated an siRNA-resistant ATP synthase β construct by altering the codons without changing the amino acid residues in the siRNA target sequences. Fig. 7 A shows that robust expression of this construct is observed in the presence of siRNA compared with that of the nonresistant construct. We generated siRNA-resistant Lys 259 and Lys 480 mutants by changing the individual Lys to Arg or Gln. The Lys to Arg mutation is considered to mimic the deacetylated state, whereas the Lys to Gln mutation abolishes the positive charge and mimics the acetylated state (Schwer et al., 2006; Tao et al., 2010). Because of the limited amount of mitochondria obtained from the transfected cells, we used a commercially available assay for measuring complex V activity described in detail in the Materials and methods section. Using this assay, we determined the activity of the Lys 259 and Lys 480 variants. Fig. 7 B shows that K259R and K480R mutants have a 70–80% increase in activity, whereas K259Q and K480Q have an ∼40% decrease in activity compared with that of the control. We also generated double mutants that mimic the deacetylated state (K259/480R), which show a further increase (150%) in activity, whereas double mutants that mimic the acetylated state (K259/480Q) show a 75–80% decrease in activity compared with that of the control. These results indicate that complex V activity correlates with the acetylation state of ATP synthase β. These results are consistent with a model proposing that SIRT3 regulates this process by deacetylating Lys 259 and Lys 480.

To understand how these Lys residues could affect the catalytic activity of ATP synthase β, we examined the crystal structure of the bovine F1–stator complex in different conformational states: nucleotide free or bound to adenylyl imidodiphosphate, ADP, or ADP with the transition state mimetic aluminum fluoride (Abrahams et al., 1994; Menz et al., 2001; Rees et al., 2009). Lys 259 (Lys 206, based on crystal structure labeling) identified in our study is located in a surface-exposed loop in all three states (Fig. 7 C). This loop connects to helix C, which follows the loop containing β–Glu 188 and β–Arg 189, and contacts α–Arg 373. All three residues are essential for catalysis (Menz et al., 2001). β–Glu 188 directly interacts with the nucleophilic water molecule that attacks the terminal phosphate of ATP during hydrolysis. β–Arg 189 is involved in the direct binding of the γ phosphate, and α–Arg 373 in the α chain is a critical residue, termed an arginine finger, which contributes to catalysis by accelerating the rate of ATP cleavage by stabilizing the transition state of ATP hydrolysis. Thus, acetylation of Lys 206 could potentially lead to conformational changes in the active site region and affect the positioning of β–Glu 188, β–Arg 189, and α–Arg 373. Lys 480 (Lys 430 in the crystal structure), the second lysine identified in our study as a target for the *Drosophila* Sirt2 deacetylase, is in a loop that packs over the base moiety of the nucleotide in the active site region in the nucleotide-bound states. Notably, the backbone of Lys 430 mediates hydrogen bonding interactions with the backbone of Phe 418, which makes van der Waals contacts with the base. Lys 430 is involved in an intramolecular interaction with Glu 465. Acetylation of Lys 430 could disrupt this salt bridge interaction and potentially induce a conformational change in the nucleotide-binding region. These structural observations suggest that acetylation of Lys 259 and Lys 480 in ATP synthase β affects protein conformation near the active site, thereby leading to decreased catalytic activity.

Inverse correlation between acetylation of ATP synthase β and complex V activity in human cancer cell lines

We finally assessed the pathophysiological implications of acetylation of ATP synthase β. The prevalence of acetyl modifications in mitochondrial proteins that affect energy metabolism suggests that altered acetylation could potentially contribute to diseases such as cancer and cardiac dysfunction, which exhibit recognizable changes in energy metabolism. For these experiments, we chose three human breast cancer cell lines with different invasive potential: T47D, MDA-MB-435, and MDA-MB-231. T47D cells are more differentiated, weakly invasive, and rely less on aerobic glycolysis for energy compared with MDA-MB-231 cells, which are less differentiated, strongly invasive, and have increased reliance on glycolysis for energy generation. We immunoprecipitated endogenous ATP synthase β from these cells and probed them with the acetyl-Lys antibody. ATP synthase β is less acetylated in T47D cells compared with those of

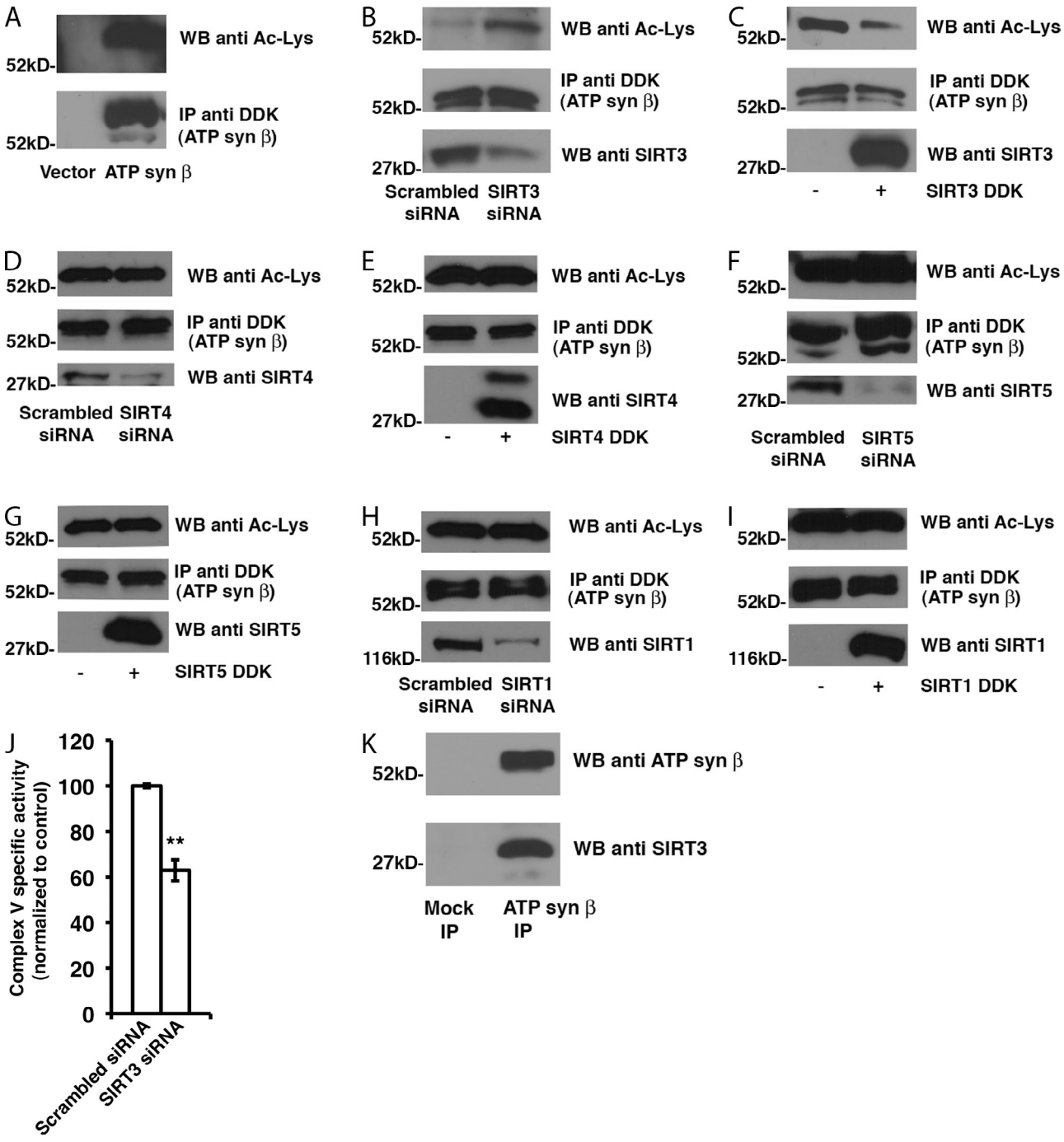

Figure 6. **Human ATP synthase β is an acetylated protein, and its deacetylation is regulated by SIRT3.** (A) pCMV vector or ATP synthase β (DDK tagged) was transfected in HEK293T cells, immunoprecipitated using an antibody to DDK tag, and probed with an antibody to acetyl-Lys (Ac-Lys). (B) HEK293T cells were cotransfected with ATP synthase β (ATP syn β) and either SIRT3 siRNA or scrambled siRNA. ATP synthase β was immunoprecipitated, and its acetylation status was assessed. The bottom blot shows reduction of SIRT3 protein upon siRNA treatment. Knockdown of SIRT3 increases acetylation of ATP synthase β. (C) Expression vector for wild-type SIRT3 was cotransfected in HEK293T cells with ATP synthase β, and its acetylation status was assessed after immunoprecipitation. Overexpression of SIRT3 decreases acetylation of ATP synthase β. (D) HEK293T cells were cotransfected with ATP synthase β and either SIRT4 siRNA or scrambled siRNA. SIRT4 knockdown does not affect acetylation of ATP synthase β. (E) Wild-type SIRT4 expression vector was cotransfected in HEK293T cells with ATP synthase β, and its acetylation status was assessed after immunoprecipitation. SIRT4 overexpression does not affect acetylation of ATP synthase β. (F) HEK293T cells were cotransfected with ATP synthase β and either SIRT5 siRNA or scrambled siRNA. SIRT5 knockdown does not affect acetylation of ATP synthase β. (G) Wild-type SIRT5 expression vector was cotransfected in HEK293T cells with ATP synthase β, and its acetylation status was assessed after immunoprecipitation. SIRT5 overexpression does not affect acetylation of ATP synthase β. (H) HEK293T cells were cotransfected with ATP synthase β and either SIRT1 siRNA or scrambled siRNA. SIRT1 knockdown does not affect acetylation of ATP synthase β. (I) Wild-type SIRT1 expression vector was cotransfected in HEK293T cells with ATP synthase β, and its acetylation status was assessed after immunoprecipitation. SIRT1 overexpression does not affect acetylation of ATP synthase β. (J) Mitochondria were prepared from SIRT3 siRNA–treated or scrambled siRNA–treated cells, and complex V activity was measured. The activity of mitochondria from scrambled siRNA treatment was taken as 100%. SIRT3 knockdown results in an ~40% decrease in complex V activity. $n = 3$; error bars represent SDs. **, $P \leq 0.01$–0.001 in Student's t test. (K) Endogenous ATP synthase β was immunoprecipitated from HEK293T cells overexpressing SIRT3, and the immunoprecipitate was probed with antibodies to ATP synthase β and SIRT3. SIRT3 can coimmunoprecipitate with ATP synthase β. IP, immunoprecipitation; WB, Western blot.

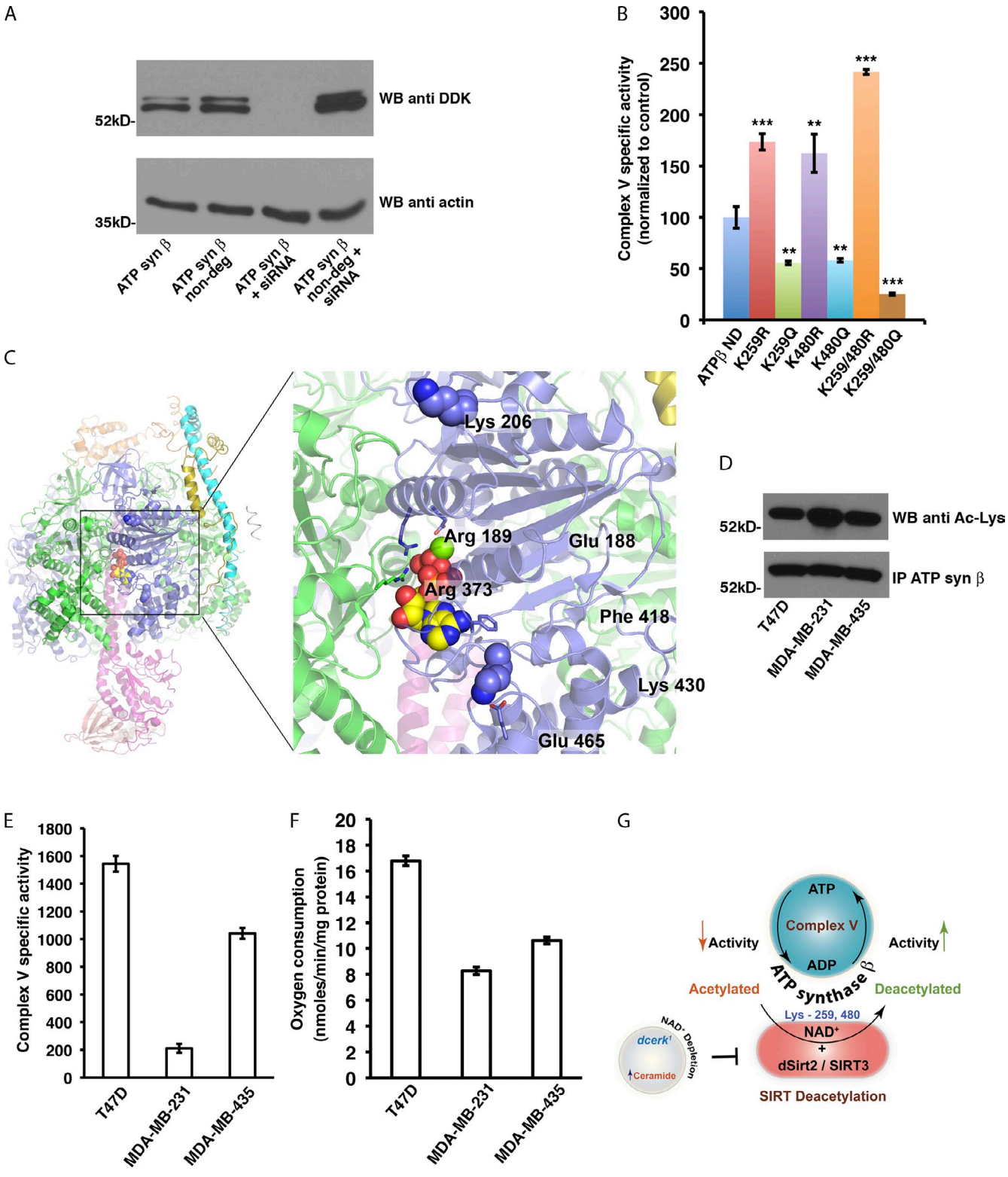

Figure 7. **Acetylation of ATP synthase β at Lys 259 and Lys 480 regulates complex V activity.** (A) Nondegradable (non-deg) ATP synthase β (ATP syn β) is resistant to targeted siRNA-mediated degradation. (B) siRNA-resistant versions of ATP synthase β wherein Lys 259 or Lys 480 either individually or together were substituted with Arg or Gln and cotransfected with siRNA to ATP synthase β. Mitochondria were prepared, and complex V activity was measured using an immunocapture assay followed by the amount of ATP synthase β in the same samples. The activity of siRNA-resistant ATP synthase β is taken as 100%. Substitution of either Lys or both with Arg results in increased activity, whereas substitution with Gln results in decreased complex V activity. **, $P \leq 0.01$–0.001; ***, $P \leq 0.001$–0.0001. (C) An overview of the crystal structure of bovine mitochondrial F1–stator complex is shown on the left in ribbon representation. The F1 domain contains 3α (green), 3β (purple), and a single subunit of γ (pink). The stator complex shows portions of subunit b (teal), oligomycin sensitivity-conferring protein (orange), and F6 (yellowish green). The right shows a closer view of the region around the active site (marked by the black box in the left image). The Lys residues are shown as spheres, and the active site amino acids are shown as stick models. Acetylation of Lys 259 (Lys 206 in the crystal structure) and Lys 480 (430 in the crystal structure) could affect protein conformation near the active site.

MDA-MB-435 and MDA-MB-231 cells, which show the most acetylation (Fig. 7 D). We prepared mitochondria from these cells and measured complex V activity and oxygen consumption rates. Complex V is more active in T47D cells compared with those of MDA-MB-435 and MDA-MB-231 cells (Fig. 7 E). T47D cells also show a higher oxygen consumption rate than MDA-MB-231 (Fig. 7 F). There appears to be an inverse correlation between acetylation of ATP synthase β and complex V activity in these cell lines.

Discussion

In this study, we demonstrate that ATP synthase β is an acetylated protein, and its deacetylation is regulated by *Drosophil*a Sirt2/mammalian SIRT3. Deacetylation of Lys 259 and Lys 480 leads to increased enzyme activity of complex V. The activity of complex V is reduced when ATP synthase β is hyperacetylated, which occurs in *Drosophila sirt2* mutants or in a human cell line when SIRT3 expression is reduced. We demonstrate that a novel ceramide–NAD^+–sirtuin axis exists by linking increased ceramide levels to altered NAD^+ levels and sirtuin activity in *dcerk*^{1} mutants. These results are summarized in the model depicted in Fig. 7 G. During the course of this study, we identified the *Drosophila* mitochondrial acetylome and determined potential substrates for dSirt2.

Although sphingolipids been extensively studied, a connection between enzymes and metabolites of this pathway and protein acetylation/deacetylation or the effects of sphingolipids on NAD^+ metabolism and sirtuins are largely unexplored. Our observations in *dcerk*^{1} mutants set the stage to further explore the sphingolipid–NAD–sirtuin axis and delineate links between sphingolipid metabolites and NAD metabolism. Although the reason for depletion of NAD^+ is not clear, the increased glycolysis and decreased OXPHOS observed in *dcerk*^{1} would accentuate this decrease. NAD^+ has been proposed as an attractive target in the management of various pathologies, particularly in the prevention of aging and related disorders, such as diabetes, obesity, and cancer (Yoshino et al., 2011; Houtkooper and Auwerx, 2012). Many sphingolipids, including ceramide, are altered in obesity, diabetes, and aging (Russo et al., 2013). Further studies should help us decipher whether changes in the sphingolipid–NAD axis contribute to stress-associated pathologies observed in these conditions.

Recent global proteomic surveys involving mitochondrial acetylation have focused on liver tissue from wild-type and *Sirt3*$^{-/-}$ mice and embryonic fibroblasts derived from these mice (Sol et al., 2012; Hebert et al., 2013; Rardin et al., 2013). Our proteomic study using mitochondria from wild-type and *dsirt2* flies provides the first inventory of acetylated proteins and sites in *Drosophila* mitochondria. In addition to complementing the mouse studies, the availability of the *Drosophila* data will enable the use of the *Drosophila* model for evaluation of several site-specific Lys variants in different proteins. It will facilitate studies of tissue-specific expression of constitutively acetylated or deacetylated mutants, and the phenotypic consequences observed in these studies would lead to an understanding of the role of site-specific modifications in vivo. Enzymes involved in the TCA cycle, OXPHOS, β-oxidation of fatty acids, and branched-chain amino acid catabolism, which are enriched in the mouse acetylome, are also enriched in the *Drosophila* acetylome. These results indicate a high degree of conservation of mitochondrial acetylation. Analyses of the *sirt2* acetylome reveal that many proteins that are hyperacetylated in *dsirt2* mutants are also hyperacetylated in liver from *Sirt3*$^{-/-}$ mice, and some of these candidates have been validated as substrates of SIRT3. These results along with phenotypes, related to mitochondrial dysfunction, observed in the *dsirt2* mutants (increased ROS levels, decreased oxygen consumption, decreased ATP level, and increased sensitivity to starvation) strengthen the idea that dSirt2 serves as a functional homologue of mammalian SIRT3. For any organism, tight regulation of ATP synthase activity is crucial to meet physiological energy demands in quickly changing nutritional or environmental conditions. Sirtuins regulate reversible acetylation under stress conditions. It is conceivable that acetylation-mediated regulation of complex V could constitute part of an elaborate control system.

Cancer cells generate a greater proportion of ATP via glycolysis instead of OXPHOS, a phenomenon called the Warburg effect (Warburg, 1956). Recent studies show that SIRT3 dysfunction could be an important factor in this metabolic reprogramming (Kim et al., 2010; Finley et al., 2011a). Thus, alterations in mitochondrial acetylation states could contribute to the preference for aerobic glycolysis observed in cancer. Our results with human breast cancer cell lines show that ATP synthase β is more acetylated in MDA-MB-231 cells (which are less differentiated, strongly invasive, and more glycolytic) compared with that in T47D cells (which are more differentiated, less invasive, and less reliant on aerobic glycolysis). It would be interesting to address whether the acetylation status of ATP synthase β could contribute to the pathological shift in energy generation observed in cancer cells. In conclusion, our study has identified a ceramide–NAD^+–sirtuin connection in *Drosophila* and has shown that deacetylation of the ATP synthase β subunit mediated by *Drosophila* Sirt2/mammalian SIRT3 adds a new layer of regulation of mitochondrial complex V activity.

(D) Endogenous ATP synthase β was immunoprecipitated from human breast cancer cell lines, and its acetylation status was assessed using an acetyl-Lys antibody. ATP synthase β is more acetylated in MDA-MB-231 cells compared with T47D. (E) Complex V activity was measured in mitochondria prepared from human breast cancer cell lines. The activity is significantly less in MDA-MB-231 cells compared with that in T47D cells. $n = 3$. Analysis of variance was performed, and Tukey's honest significance test was applied to determine significance. T47D–MDA-MB-231: adjusted $P = 1.0 \times 10^{-7}$; T47D–MDA-MB-435: adjusted $P = 1.9 \times 10^{-5}$. (F) Oxygen consumption is less in MDA-MB-231 compared with that in T47D mitochondria. $n = 3$. Analysis of variance was performed, and Tukey's honest significance test was applied to determine significance. T47D–MDA-MB-231: adjusted $P = 2.0 \times 10^{-6}$; T47D–MDA-MB-435: adjusted $P = 1.0 \times 10^{-5}$. (G) A model depicting *Drosophila* Sirt2/mammalian SIRT3-mediated deacetylation of ATP synthase β and its impact on complex V activity. Error bars represent SDs. IP, immunoprecipitation; WB, Western blot.

Materials and methods

Fly stocks

Drosophila stocks were raised on standard corn meal agar and maintained at 25°C. *dcerk*^{1} is a severe hypomorphic allele generated by *P* element excision and characterized as previously described (Dasgupta et al., 2009). *dsir2*, *sirt2*, *sirt4*, and *sirt7* mutant flies and the actin-GAL4 driver were obtained from Bloomington Stock Center (Indiana University). The upstream activation sequence (UAS)–dSirt2 transgene was a gift from K. Chang (University of Southern California, Los Angeles, CA). The UAS RNAi line for dSirt6 was obtained from the Vienna Drosophila RNAi Center. *dcerk*^{1}*.dsirt2* double mutants were generated by meiotic recombination, loss of ceramide kinase was confirmed by Western blotting, and absence of Sirt2 was confirmed by quantitative PCR. For rescue experiments, *dcerk*^{1} mutants were recombined to UAS-dSirt2 transgenic flies, and *dsirt2* mutants were also recombined to UAS-dSirt2 transgenic flies.

Isolation of mitochondria

Approximately 1,000 flies were homogenized in mitochondrial isolation buffer containing 250 mM sucrose, 10 mM Tris, pH 7.4, and 0.15 mM $MgCl_2$ with a pestle and mortar. The homogenate was centrifuged at 4,000 *g* for 15 min at 4°C and then passed through an acrodisc syringe filter (0.45-µm pore size). The supernatant was centrifuged at 16,000 *g* for 30 min to obtain a mitochondria-enriched pellet. The supernatant was recentrifuged at 16,000 *g* for 15 min, and the pellets were pooled, washed, and resuspended in isolation buffer for activity measurements. Mitochondrial enrichment was assessed by Western blotting the extract with an antibody to porin, a mitochondrial marker.

Assay of complex V (ATPase) activity

The assay relies on linking the ATPase activity to NADH oxidation via the conversion of phosphoenolpyruvate to pyruvate by pyruvate kinase and then pyruvate to lactate by lactate dehydrogenase. The reaction buffer consisted of 250 mM sucrose, 50 mM KCl, 5 mM $MgCl_2$, 2 mM KCN, and 20 mM Tris-HCl, pH 7.5. Before the test, 0.25 mM NADH, 1 mM phosphoenol pyruvate, 2.5 U/ml lactate dehydrogenase, and 2 U/ml pyruvate kinase were added to the reaction buffer. The reaction was started by adding 40 µg *Drosophila* mitochondria, and the change in absorbance was recorded over 3 min at 340 nm. To determine the oligomycin-sensitive activity, the experiment was repeated with 6 µg/ml oligomycin. Complex V activity was calculated by using the extinction coefficient 6.22 $mM^{-1}cm^{-1}$.

Metabolic profiling

For measurement of NAD^+ and related metabolites, *dcerk*^{1} and *w*^{1118} (100 flies each, in triplicate) were collected and frozen. The samples were prepared and analyzed by LC-MS, LC-MS/MS, and gas chromatography–MS platforms by Metabolon.

Feeding experiments

For feeding experiments, 1-d-old *w*^{1118} or *dcerk*^{1} flies were transferred to fly food containing 50 mM nicotinamide or 10 mM NAD^+. 1,000 flies were used (40 flies per vial) in each feeding experiment. After 24 h, the flies were transferred to vials containing fresh nicotinamide or NAD^+. The flies were collected after 48 h, and mitochondria were prepared in the presence of nicotinamide or NAD^+ and assayed for mitochondrial complex V activity.

Mitochondrial oxygen consumption

The rate of oxygen consumption was measured using a Clark-type electrode. Freshly isolated mitochondria (0.5 mg/ml) were incubated in assay medium (120 mM KCl, 5 mM KH_2PO_4, 3 mM Hepes, 1 mM EGTA, 1 mM $MgCl_2$, and 0.2% bovine serum albumin, pH 7.2) supplemented with a mixture of 20 mM sodium pyruvate and 20 mM proline as a substrate. State 3 rates were measured after the addition of 2 mM ADP.

Mitochondrial ROS production

The rate of mitochondrial H_2O_2 production was assayed fluorometrically by measuring the increase in fluorescence (excitation at 312 nm and emission at 420 nm) as a result of oxidation of homovanillic acid by H_2O_2 in the presence of HRP. Freshly isolated mitochondria (0.2 mg/ml) were incubated in 2 ml assay medium containing 0.1 mM homovanillic acid and 6 U/ml HRP. After a steady signal was obtained, substrate was added: either 5 mM pyruvate + 5 mM proline or 20 mM *sn*-glycerol 3-phosphate followed by 5 µM rotenone.

BN-PAGE

Mitochondria were prepared from flies in the presence of 10 mM nicotinamide and 500 nM trichostatin A and resuspended in buffer containing 20 mM Bis-Tris, pH 7.0, 50 mM NaCl, 2 mM 6-aminohexanoic acid, and 1 mM EDTA. 400 µg mitochondria was solubilized by adding 20% digitonin corresponding to digitonin/protein ratios ranging from 4 to 6 g/g. The samples were incubated for 30 min at 4°C and then centrifuged for 20 min at 16,000 *g*. The supernatant was separated by BN-PAGE at room temperature after addition of 5 µl of 50% glycerol and 3 µl Coomassie blue G-250 dye from a 5% suspension in 500 mM 6-aminohexanoic acid (Wittig et al., 2006). 4–12% gradient acrylamide gels were used for separation of the digitonin-solubilized respiratory complexes. The cathode buffer was 50 mM tricine, 15 mM Bis-Tris, pH 7.0, and 0.02% Serva blue G-250 (wt/vol), and the anode buffer was 50 mM Bis-Tris, pH 7.0. The gels were stained with Coomassie brilliant blue R-250 followed by destaining in a solution containing 10% methanol and 8% acetic acid, or in-gel activity assays were performed for mitochondrial protein complexes II–V.

In-gel activity staining of OXPHOS complexes was performed as follows: For complex II staining, the gel strip was incubated in 20 ml of 5-mM Tris-HCl, pH 7.4, containing 0.5 M sodium succinate, 215 mM phenazine methosulfate, and 20 mg nitrotetrazolium blue. Staining of complex III was achieved by incubating the gel strip in 50 ml complex III assay buffer containing 50 mM potassium phosphate buffer, pH 7.4, and 20 mg DAB. After the color developed (~6 h), the gel was scanned and then put back in the assay buffer, and 50 mg cytochrome *c* was added to start the complex IV assay and stained for ~1 h. For complex V staining, the gel strip was incubated overnight in a 50-ml solution containing 35 mM Tris-HCl, pH 8.0, 270 mM glycine, 14 mM $MgSO_4$, 8 mM ATP, and 0.3% (wt/vol) $Pb(NO_3)_2$ with slow agitation. All steps were conducted at room temperature, and the reactions were stopped after the color was developed by fixing the gel for 30 min in a solution containing 50% methanol (vol/vol) and 10% acetic acid (vol/vol).

Sample preparation, MS, and data analysis

Bands corresponding to different OXPHOS complexes were excised from BN-PAGE gels and digested with trypsin. The peptides were desalted and subjected to LC-MS/MS using a mass spectrometer (LTQ Orbitrap Velos Pro with Proxeon Easy LC; Thermo Fisher Scientific), and the spectra were evaluated using SORCERER 2. For identification of the mitochondrial acetylome, mitochondria were prepared from *w*^{1118} flies in duplicate (~3,000 flies/batch). For identification of *dsirt2* acetylome, mitochondria were prepared similarly from *dsirt2* mutant flies. The acetyl scans were performed at Cell Signaling Technology. Mitochondria were digested with trypsin, and acetyl-Lys peptide enrichment was performed using the acetyl-Lys motif antibody (#9895; Cell Signaling Technology). The LC-MS/MS analysis was performed using electrospray ionization–collision induced dissociation (LTQ Orbitrap Velos). The acetyl-Lys–enriched peptides were loaded directly onto a 10-cm × 75-µm capillary column (PicoFrit; New Objective) packed with reversed-phase resin (Magic C18 AQ; Michrom Bioresources). The column was developed with a 90-min linear gradient of acetonitrile in 0.125% formic acid delivered at 280 nl/min.

MS parameter settings. The MS run time was 96 min, MS1 scan range was 300.00–1,500.00, and the top 20 MS/MS has a minimum signal of 500. Isolation width was 2.0, normalized collision energy was 35.0, activation Q was 0.250, activation time was 20.0, and lock mass was 371.101237. Charge state rejection parameter was enabled, and a charge state of 1+ was rejected. Dynamic exclusion was enabled, the repeat count was 1, repeat duration was 35.0, exclusion list size was 500, and exclusion duration was 40.0. Exclusion mass width was relative to mass, and exclusion mass width was 10 ppm.

Informatics. MS/MS spectra were evaluated using SEQUEST 3G and the SORCERER 2 platform obtained from Sage-N Research (v4.0; Lundgren et al., 2009). Searches were performed against the most recent update of the NCBI *Drosophila* database with a mass accuracy of ±50 ppm for precursor ions and 1 D for product ions. Results were filtered with a mass accuracy of ±5 ppm on precursor ions and the presence of the intended motif.

Bioinformatics

Enriched GO analysis and pathway analysis were performed using the ChIPpeakAnno package from Bioconductor (Zhu, et al., 2010). GO terms and pathways were annotated with at least five genes in the genome, and Benjamini and Hochberg–adjusted $P < 0.01$ was considered significantly enriched (Benjamini and Hochberg, 1995). Amino acid sequences were obtained using the biomaRt package obtained from Bioconductor (Durinck,

et al., 2005). Consensus amino acid patterns surrounding acetyl-Lys sites (±6 amino acids) were identified ($P < 0.05$) and visualized using iceLogo with nonacetylated lysines of all acetylated mitochondria proteins as the background model (Colaert, et al., 2009).

Cell culture and transfection experiments

Transfection was performed using the nucleofection device (Amaxa Nucleofector; Lonza) and reagents according to the manufacturer's standard protocol. In brief, HEK293T cells were cultured in DMEM (10% FBS + 1% penicillin-streptomycin) 3 d before the experiment. 5×10^5 cells were used for each nucleofection. The cell pellet was resuspended in 100 µl nucleofection solution and then added to the total plasmid DNA (3 µg). The cell DNA mixture in a 1-cm cuvette is nucleoporated according to a predefined program (A-023). After electroporation, cells were incubated in media with 10 mM nicotinamide and 500 nM trichostatin A unless otherwise mentioned. Cells are harvested after 24 h for immunoprecipitation. DDK-tagged (similar to FLAG tag) ATP synthase β (RC201638) and DDK-tagged human SIRT3 (RC200190), SIRT4 (RC212226), SIRT5 (RC200189), and SIRT1 (RC218134) plasmids were obtained from OriGene. In deacetylation experiments involving SIRT3 overexpression, DDK-tagged human SIRT3 was cotransfected with DDK-tagged ATP synthase β, and cells were incubated in media without nicotinamide and trichostatin A. For siRNA experiments, cells were transfected with each siRNA (1 µM) or the scrambled version, and cells were harvested after 72 h. The Trilencer siRNAs used to reduce SIRT3 (SR308255), SIRT4 (SR308254), SIRT5 (SR308253), SIRT1 (SR308256), and the scrambled siRNAs were obtained from OriGene. The siRNA sequences used to reduce endogenous ATP synthase β were 5′-CUGCAUUAUUGGGCCGAAU-3′ and 5′-AAUCAACAAUGUCGCCAAA-3′ (Thermo Fisher Scientific).

Immunoprecipitation and immunoblotting

After transfection, cells were lysed in radioimmunoprecipitation assay buffer with protease inhibitor cocktail (Roche). DDK-tagged proteins were immunoprecipitated using a DDK antibody (mouse), 4C5, coupled to protein G–agarose beads (OriGene). The immunoprecipitate was washed in radioimmunoprecipitation assay buffer and dissolved in SDS sample buffer. For immunoprecipitation of endogenous ATP synthase β, either HEK293T or human breast cancer cells were lysed in NP1 buffer (PBS with 0.5% Nonidet P-40) and protease inhibitor cocktail. The extract is incubated for 8–10 h at 4°C with an antibody to ATP synthase β (MitoSciences) or IgG (mock) followed by addition of immobilized protein G (Thermo Fisher Scientific) and incubated further for 12 h at 4°C. The beads were centrifuged at 5,000 rpm for 5 min and washed three times in NP1 buffer. The beads were then incubated with 2× SDS sample buffer without β-mercaptoethanol for 10 min at room temperature. The beads were centrifuged, and the supernatant was separated by SDS-PAGE after addition of β-mercaptoethanol. For Western blotting, mouse anti-DDK antibody (OriGene) was used at 1:2,000, mouse anti-ATP synthase β was used at 1:4,000 (MitoSciences), and rabbit anti–human SIRT3 antibody (Cell Signaling Technology) was used at 1:1,000. HRP-conjugated rabbit or mouse secondary antibodies (Jackson ImmunoResearch Laboratories, Inc.) were used at 1:5,000 dilution. For Western blot analysis, the rabbit anti–acetyl-Lys antibody (Cell Signaling Technology) was used at 1:500, and the HRP-conjugated rabbit secondary antibody was used at a 1:3,000 dilution. The blotting was performed following a published protocol (Guan et al., 2010).

Plate assay for measuring complex V activity

An siRNA-resistant ATP synthase β was synthesized by making the following changes to 5′-TTGATTAATAACGTTGCA-3′ (corresponding to amino sequence LINNVA) and 5′-AGTGCTCTGCTCGGAAGG-3′ (corresponding to amino acid sequence SALLGR). Either the nondegradable wild-type construct or each of the nondegradable site-specific Lys substitutions was transfected along with the siRNAs. Cells were harvested after 75 h, and mitochondrial-enriched fractions were prepared. The two-step complex V assay was performed using the ATP synthase-specific activity microplate assay kit according to the manufacturer's instructions (MS543; MitoSciences). In this assay, the F0F1-ATPase holoenzyme is immunocaptured within the wells of a 96-well microplate that is coated with an antibody that recognizes all subunits of the complex. The enzymatic hydrolysis of ATP to ADP is coupled to the oxidation of NADH to NAD^+, which results in a decrease in absorbance at 340 nm. Subsequently, in the same wells, the quantity of ATP synthase β is determined by adding an ATP synthase β antibody conjugated with alkaline phosphatase. An increase in absorbance at 405 nm is measured, and this is proportional to the amount of ATP synthase β captured in the wells. The ratio of activity to quantity represents the relative specific activity of ATP synthase β. The mitochondrial extract was solubilized with digitonin, and 40–60 µg was used per well. The plate was read using a microplate reader (Infinite M200 Pro; Tecan). Specific activity was taken as the ratio of complex V activity to quantity of ATP synthase β in each well.

Structural observations of ATP synthase β

The structure of the F1–stator complex was generated with PyMOL (DeLano Scientific LLC) using the bovine F1–stator complex structure.

Preparation of soluble and nuclear extracts

Soluble extracts were prepared from w^{1118} and $dcerk^1$ flies by washing them with buffer (50 mM Tris, pH 7.5, 1 mM EDTA, 2 mM β-mercaptoethanol, 50 mM KCl, 10 mM nicotinamide, and 500 nM trichostatin A) followed by homogenization in the same buffer. The homogenate was clarified by a 15-min centrifugation at 12,000 *g*, and then, the supernatant was centrifuged at 150,000 *g* for 1 h at 4°C (Malcovati et al., 1973). For preparation of nuclear extracts, flies are ground in 10 mM Tris-Cl buffer, pH 8.0, containing 300 mM sucrose, 2 mM magnesium acetate, 3 mM $CaCl_2$, 0.1% Triton X-100, 0.5 mM DTT, 10 mM nicotinamide, and 500 nM trichostatin A. The homogenate is filtered through two sheets of 100-µm nylon mesh to remove large debris. Filtrates are transferred to a Teflon/glass homogenizer and stroked 40 times on ice. Homogenates are filtered through two sheets of 35-µm nylon mesh twice and then mixed with 10 mM Tris-Cl buffer, pH 8.0, containing 1.75 M sucrose, 5 mM magnesium acetate, 0.5 mm DTT, 10 mM nicotinamide, and 500 nM trichostatin. The mixture is then divided into two equal portions and is layered over a sucrose gradient consisting of 8 ml of 10-mM Tris-Cl buffer, pH 8.0, containing 1.9 M sucrose, 5 mM magnesium acetate, and 0.5 mM DTT over 4 ml of 10-mM Tris-Cl buffer, pH 8.0, containing 25% glycerol, 5 mM magnesium acetate, 5 mM DTT, 0.1 mM EDTA, 10 mM nicotinamide, and 500 nM trichostatin A in tubes of a rotor (SW 28; Beckman Coulter). The sample is then spun at 14,000 rpm for 15 min at 4°C. The supernatant is discarded, and residual supernatant is removed with a Kimwipe. Each pellet is resuspended in 500 µl of 10-mM Tris-Cl buffer, pH 8.0, containing 25% glycerol, 5 mM magnesium acetate, 5 mM DTT, 0.1 mM EDTA, 10 mM nicotinamide, and 500 nM trichostatin A, and the suspension is spun for 1 min at maximum speed. Nuclei are recovered as a pellet (Hirayoshi and Lis, 1999).

Ceramide estimation

Sphingolipid-enriched fractions were prepared from mitochondria isolated from w^{1118} or $dcerk^1$ flies. Mitochondria were homogenized in 2.0 ml methanol/chloroform (2:1) using a Teflon homogenizer in a glass tube followed by 500 µl of water and vortexed. The homogenate was sonicated in a water bath–type sonicator for 20 min and incubated for 2 h at 37°C. To the extract, 1 ml of water and 500 µl chloroform were added, vortexed, and centrifuged at 1,000 rpm for 10 min at room temperature. The organic phase was collected and dried under nitrogen. Extracts were redissolved in 2 ml of synthetic upper (methanol/water/chloroform of 94:96:6) and applied to a pretreated column for solid-phase extraction (Sep-Pak C18; Waters Corporation). The column was washed with 4 ml of water, and lipids were extracted in 4 ml methanol followed by 4 ml methanol/chloroform. The samples were dried under nitrogen and redissolved in the requisite amount of chloroform/methanol (1:1). The d14 sphingoid base containing ceramides was estimated by ultra-HPLC/MS (Dasgupta et al., 2009, Yonamine et al., 2011).

Measurement of citrate synthase activity

Citrate synthase activity was measured by following the decrease in absorbance at 412 nm because of the reduction of DTNB (5, 5′-dithiobis-(2-nitro-benzoic acid)). The reaction mixture containing 0.1 M Tris-HCl, pH 8.0, 0.3 mM acetyl-CoA, 0.1 mM DTNB, and 10 µg mitochondrial protein was incubated for 10 min. The reaction was initiated by adding 0.5 mM oxaloacetate, and the change in absorbance was monitored for 3 min. Citrate synthase activity was calculated by using an extinction coefficient of 13.6 $mM^{-1}cm^{-1}$.

Online supplemental material

Fig. S1 shows that the NAD^+ level is decreased in the $cdase^1$ mutant. Fig. S2 shows separation of OXPHOS complexes by BN-PAGE. Fig. S3 depicts that *dsirt2* and $dcerk^1$ mutants show increased ROS levels. Fig. S4 shows a strategy for identification of *Drosophila* mitochondrial acetylome and dSirt2-regulated acetylome. Table S1 shows details of acetyl-Lys peptides in the mitochondrial acetylome identified by MS. Table S2 shows

details of acetyl-Lys peptides that increase in *dsirt2* mutant mitochondrial acetylome identified by MS. Online supplemental material is available at http://www.jcb.org/cgi/content/full/jcb.201404118/DC1.

We thank Dr. Karen Chang, the Bloomington Stock Center, and the Vienna Drosophila RNAi Center for fly stocks. We thank Dr. Corey Smith in the Kaufman laboratory for helpful discussions on preparation of nuclear extracts. We are grateful to the Urano laboratory and Dr. Amartya Sanyal for help with nucleofection experiments. We thank the Torres laboratory for generous access to the microplate reader. We thank Kathya Acharya for help with figures.

This research is supported by a National Institutes of Health grant (RO1EY016469) to U.R. Acharya.

The authors declare no competing financial interests.

Submitted: 22 April 2014
Accepted: 10 June 2014

References

Abrahams, J.P., A.G. Leslie, R. Lutter, and J.E. Walker. 1994. Structure at 2.8 A resolution of F1-ATPase from bovine heart mitochondria. *Nature*. 370:621–628. http://dx.doi.org/10.1038/370621a0

Acharya, J.K., U. Dasgupta, S.S. Rawat, C. Yuan, P.D. Sanxaridis, I. Yonamine, P. Karim, K. Nagashima, M.H. Brodsky, S. Tsunoda, and U. Acharya. 2008. Cell-nonautonomous function of ceramidase in photoreceptor homeostasis. *Neuron*. 57:69–79. http://dx.doi.org/10.1016/j.neuron.2007.10.041

Ahn, B.H., H.S. Kim, S. Song, I.H. Lee, J. Liu, A. Vassilopoulos, C.X. Deng, and T. Finkel. 2008. A role for the mitochondrial deacetylase Sirt3 in regulating energy homeostasis. *Proc. Natl. Acad. Sci. USA*. 105:14447–14452. http://dx.doi.org/10.1073/pnas.0803790105

Banerjee, K.K., C. Ayyub, S.Z. Ali, V. Mandot, N.G. Prasad, and U. Kolthur-Seetharam. 2012. dSir2 in the adult fat body, but not in muscles, regulates life span in a diet-dependent manner. *Cell Reports*. 2:1485–1491. http://dx.doi.org/10.1016/j.celrep.2012.11.013

Benjamini, Y., and Y. Hochberg. 1995. Controlling the false discovery rate: a practical and powerful approach to multiple testing. *J. R. Stat. Soc., B*. 57:289–300.

Bikman, B.T., and S.A. Summers. 2011. Ceramides as modulators of cellular and whole-body metabolism. *J. Clin. Invest.* 121:4222–4230. http://dx.doi.org/10.1172/JCI57144

Boyer, P.D. 1997. The ATP synthase—a splendid molecular machine. *Annu. Rev. Biochem.* 66:717–749. http://dx.doi.org/10.1146/annurev.biochem.66.1.717

Campesan, S., E.W. Green, C. Breda, K.V. Sathyasaikumar, P.J. Muchowski, R. Schwarcz, C.P. Kyriacou, and F. Giorgini. 2011. The kynurenine pathway modulates neurodegeneration in a *Drosophila* model of Huntington's disease. *Curr. Biol.* 21:961–966. http://dx.doi.org/10.1016/j.cub.2011.04.028

Chen, Y., J. Zhang, Y. Lin, Q. Lei, K.L. Guan, S. Zhao, and Y. Xiong. 2011. Tumour suppressor SIRT3 deacetylates and activates manganese superoxide dismutase to scavenge ROS. *EMBO Rep.* 12:534–541. http://dx.doi.org/10.1038/embor.2011.65

Choudhary, C., C. Kumar, F. Gnad, M.L. Nielsen, M. Rehman, T.C. Walther, J.V. Olsen, and M. Mann. 2009. Lysine acetylation targets protein complexes and co-regulates major cellular functions. *Science*. 325:834–840. http://dx.doi.org/10.1126/science.1175371

Cimen, H., M.J. Han, Y. Yang, Q. Tong, H. Koc, and E.C. Koc. 2010. Regulation of succinate dehydrogenase activity by SIRT3 in mammalian mitochondria. *Biochemistry*. 49:304–311. http://dx.doi.org/10.1021/bi901627u

Colaert, N., K. Helsens, L. Martens, J. Vandekerckhove, and K. Gevaert. 2009. Improved visualization of protein consensus sequences by iceLogo. *Nat. Methods*. 6:786–787. http://dx.doi.org/10.1038/nmeth1109-786

Dasgupta, U., T. Bamba, S. Chiantia, P. Karim, A.N. Tayoun, I. Yonamine, S.S. Rawat, R.P. Rao, K. Nagashima, E. Fukusaki, et al. 2009. Ceramide kinase regulates phospholipase C and phosphatidylinositol 4, 5, bisphosphate in phototransduction. *Proc. Natl. Acad. Sci. USA*. 106:20063–20068. http://dx.doi.org/10.1073/pnas.0911028106

Durinck, S., Y. Moreau, A. Kasprzyk, S. Davis, B. De Moor, A. Brazma, and W. Huber. 2005. BioMart and Bioconductor: a powerful link between biological databases and microarray data analysis. *Bioinformatics*. 21:3439–3440. http://dx.doi.org/10.1093/bioinformatics/bti525

Fernandez-Marcos, P.J., E.H. Jeninga, C. Canto, T. Harach, V.C. de Boer, P. Andreux, N. Moullan, E. Pirinen, H. Yamamoto, S.M. Houten, et al. 2012. Muscle or liver-specific Sirt3 deficiency induces hyperacetylation of mitochondrial proteins without affecting global metabolic homeostasis. *Sci Rep*. 2:425–433. http://dx.doi.org/10.1038/srep00425

Finley, L.W., A. Carracedo, J. Lee, A. Souza, A. Egia, J. Zhang, J. Teruya-Feldstein, P.I. Moreira, S.M. Cardoso, C.B. Clish, et al. 2011a. SIRT3 opposes reprogramming of cancer cell metabolism through HIF1α destabilization. *Cancer Cell*. 19:416–428. http://dx.doi.org/10.1016/j.ccr.2011.02.014

Finley, L.W., W. Haas, V. Desquiret-Dumas, D.C. Wallace, V. Procaccio, S.P. Gygi, and M.C. Haigis. 2011b. Succinate dehydrogenase is a direct target of sirtuin 3 deacetylase activity. *PLoS ONE*. 6:e23295. http://dx.doi.org/10.1371/journal.pone.0023295

Griswold, A.J., K.T. Chang, A.P. Runko, M.A. Knight, and K.T. Min. 2008. Sir2 mediates apoptosis through JNK-dependent pathways in *Drosophila*. *Proc. Natl. Acad. Sci. USA*. 105:8673–8678. http://dx.doi.org/10.1073/pnas.0803837105

Guan, K.L., W. Yu, Y. Lin, Y. Xiong, and S. Zhao. 2010. Generation of acetyllysine antibodies and affinity enrichment of acetylated peptides. *Nat. Protoc.* 5:1583–1595. http://dx.doi.org/10.1038/nprot.2010.117

Haigis, M.C., and D.A. Sinclair. 2010. Mammalian sirtuins: biological insights and disease relevance. *Annu. Rev. Pathol.* 5:253–295. http://dx.doi.org/10.1146/annurev.pathol.4.110807.092250

Hannun, Y.A., and L.M. Obeid. 2008. Principles of bioactive lipid signalling: lessons from sphingolipids. *Nat. Rev. Mol. Cell Biol.* 9:139–150. http://dx.doi.org/10.1038/nrm2329

Hebert, A.S., K.E. Dittenhafer-Reed, W. Yu, D.J. Bailey, E.S. Selen, M.D. Boersma, J.J. Carson, M. Tonelli, A.J. Balloon, A.J. Higbee, et al. 2013. Calorie restriction and SIRT3 trigger global reprogramming of the mitochondrial protein acetylome. *Mol. Cell*. 49:186–199.

Hirayoshi, K., and J.T. Lis. 1999. Nuclear run-on assays: assessing transcription by measuring density of engaged RNA polymerases. *Methods Enzymol.* 304:351–362. http://dx.doi.org/10.1016/S0076-6879(99)04021-5

Hirschey, M.D., T. Shimazu, E. Goetzman, E. Jing, B. Schwer, D.B. Lombard, C.A. Grueter, C. Harris, S. Biddinger, O.R. Ilkayeva, et al. 2010. SIRT3 regulates mitochondrial fatty-acid oxidation by reversible enzyme deacetylation. *Nature*. 464:121–125. http://dx.doi.org/10.1038/nature08778

Houtkooper, R.H., and J. Auwerx. 2012. Exploring the therapeutic space around NAD^+. *J. Cell Biol.* 199:205–209. http://dx.doi.org/10.1083/jcb.201207019

Houtkooper, R.H., C. Cantó, R.J. Wanders, and J. Auwerx. 2010. The secret life of NAD+: an old metabolite controlling new metabolic signaling pathways. *Endocr. Rev.* 31:194–223. http://dx.doi.org/10.1210/er.2009-0026

Imai, S., and L. Guarente. 2010. Ten years of NAD-dependent SIR2 family deacetylases: implications for metabolic diseases. *Trends Pharmacol. Sci.* 31:212–220. http://dx.doi.org/10.1016/j.tips.2010.02.003

Imai, S., C.M. Armstrong, M. Kaeberlein, and L. Guarente. 2000. Transcriptional silencing and longevity protein Sir2 is an NAD-dependent histone deacetylase. *Nature*. 403:795–800. http://dx.doi.org/10.1038/35001622

Kim, H.S., K. Patel, K. Muldoon-Jacobs, K.S. Bisht, N. Aykin-Burns, J.D. Pennington, R. van der Meer, P. Nguyen, J. Savage, K.M. Owens, et al. 2010. SIRT3 is a mitochondria-localized tumor suppressor required for maintenance of mitochondrial integrity and metabolism during stress. *Cancer Cell*. 17:41–52. http://dx.doi.org/10.1016/j.ccr.2009.11.023

Kim, S.C., R. Sprung, Y. Chen, Y. Xu, H. Ball, J. Pei, T. Cheng, Y. Kho, H. Xiao, L. Xiao, et al. 2006. Substrate and functional diversity of lysine acetylation revealed by a proteomics survey. *Mol. Cell*. 23:607–618. http://dx.doi.org/10.1016/j.molcel.2006.06.026

Kouzarides, T. 2000. Acetylation: a regulatory modification to rival phosphorylation? *EMBO J.* 19:1176–1179. http://dx.doi.org/10.1093/emboj/19.6.1176

Lombard, D.B., F.W. Alt, H.L. Cheng, J. Bunkenborg, R.S. Streeper, R. Mostoslavsky, J. Kim, G. Yancopoulos, D. Valenzuela, A. Murphy, et al. 2007. Mammalian Sir2 homolog SIRT3 regulates global mitochondrial lysine acetylation. *Mol. Cell. Biol.* 27:8807–8814. http://dx.doi.org/10.1128/MCB.01636-07

Lombard, D.B., D.X. Tishkoff, and J. Bao. 2011. Mitochondrial sirtuins in the regulation of mitochondrial activity and metabolic adaptation. *Handbook Exp. Pharmacol.* 206:163–188. http://dx.doi.org/10.1007/978-3-642-21631-2_8

Lundgren, D.H., H. Martinez, M.E. Wright, and D.K. Han. 2009. Protein identification using Sorcerer 2 and SEQUEST. *Curr. Protoc. Bioinformatics*. Chapter 13:Unit 13.3.

Luthi-Carter, R., D.M. Taylor, J. Pallos, E. Lambert, A. Amore, A. Parker, H. Moffitt, D.L. Smith, H. Runne, O. Gokce, et al. 2010. SIRT2 inhibition achieves neuroprotection by decreasing sterol biosynthesis. *Proc. Natl. Acad. Sci. USA*. 107:7927–7932. http://dx.doi.org/10.1073/pnas.1002924107

Malcovati, M., G. Valentini, and H.L. Kornberg. 1973. Two forms of pyruvate kinase in *E. coli*: their properties and regulation. *Acta Vitaminol. Enzymol.* 27:96–111.

Menz, R.I., J.E. Walker, and A.G. Leslie. 2001. Structure of bovine mitochondrial F(1)-ATPase with nucleotide bound to all three catalytic sites:

implications for the mechanism of rotary catalysis. *Cell*. 106:331–341. http://dx.doi.org/10.1016/S0092-8674(01)00452-4

Newman, J.C., W. He, and E. Verdin. 2012. Mitochondrial protein acylation and intermediary metabolism: regulation by sirtuins and implications for metabolic disease. *J. Biol. Chem.* 287:42436–42443. http://dx.doi.org/10.1074/jbc.R112.404863

Nirala, N.K., M. Rahman, S.M. Walls, A. Singh, L.J. Zhu, T. Bamba, E. Fukusaki, S.M. Srideshikan, G.L. Harris, Y.T. Ip, et al. 2013. Survival response to increased ceramide involves metabolic adaptation through novel regulators of glycolysis and lipolysis. *PLoS Genet.* 9:e1003556. http://dx.doi.org/10.1371/journal.pgen.1003556

Noji, H., R. Yasuda, M. Yoshida, and K. Kinosita Jr. 1997. Direct observation of the rotation of F1-ATPase. *Nature*. 386:299–302. http://dx.doi.org/10.1038/386299a0

Qiu, X., K. Brown, M.D. Hirschey, E. Verdin, and D. Chen. 2010. Calorie restriction reduces oxidative stress by SIRT3-mediated SOD2 activation. *Cell Metab.* 12:662–667. http://dx.doi.org/10.1016/j.cmet.2010.11.015

Rardin, M.J., J.C. Newman, J.M. Held, M.P. Cusack, D.J. Sorensen, B. Li, B. Schilling, S.D. Mooney, C.R. Kahn, E. Verdin, and B.W. Gibson. 2013. Label-free quantitative proteomics of the lysine acetylome in mitochondria identifies substrates of SIRT3 in metabolic pathways. *Proc. Natl. Acad. Sci. USA*. 110:6601–6606. http://dx.doi.org/10.1073/pnas.1302961110

Rees, D.M., A.G. Leslie, and J.E. Walker. 2009. The structure of the membrane extrinsic region of bovine ATP synthase. *Proc. Natl. Acad. Sci. USA*. 106:21597–21601. http://dx.doi.org/10.1073/pnas.0910365106

Reis, T., M.R. Van Gilst, and I.K. Hariharan. 2010. A buoyancy-based screen of *Drosophila* larvae for fat-storage mutants reveals a role for Sir2 in coupling fat storage to nutrient availability. *PLoS Genet.* 6:e1001206. http://dx.doi.org/10.1371/journal.pgen.1001206

Rosenberg, M.I., and S.M. Parkhurst. 2002. *Drosophila* Sir2 is required for heterochromatic silencing and by euchromatic Hairy/E(Spl) bHLH repressors in segmentation and sex determination. *Cell*. 109:447–458. http://dx.doi.org/10.1016/S0092-8674(02)00732-8

Russo, S.B., J.S. Ross, and L.A. Cowart. 2013. Sphingolipids in obesity, type 2 diabetes, and metabolic disease. *Handbook Exp. Pharmacol.* 216:373–401. http://dx.doi.org/10.1007/978-3-7091-1511-4_19

Sardiello, M., F. Licciulli, D. Catalano, M. Attimonelli, and C. Caggese. 2003. MitoDrome: a database of *Drosophila melanogaster* nuclear genes encoding proteins targeted to the mitochondrion. *Nucleic Acids Res.* 31:322–324. http://dx.doi.org/10.1093/nar/gkg123

Schwer, B., J. Bunkenborg, R.O. Verdin, J.S. Andersen, and E. Verdin. 2006. Reversible lysine acetylation controls the activity of the mitochondrial enzyme acetyl-CoA synthetase 2. *Proc. Natl. Acad. Sci. USA*. 103:10224–10229. http://dx.doi.org/10.1073/pnas.0603968103

Shimazu, T., M.D. Hirschey, L. Hua, K.E. Dittenhafer-Reed, B. Schwer, D.B. Lombard, Y. Li, J. Bunkenborg, F.W. Alt, J.M. Denu, et al. 2010. SIRT3 deacetylates mitochondrial 3-hydroxy-3-methylglutaryl CoA synthase 2 and regulates ketone body production. *Cell Metab.* 12:654–661. http://dx.doi.org/10.1016/j.cmet.2010.11.003

Shinmura, K., K. Tamaki, M. Sano, N. Nakashima-Kamimura, A.M. Wolf, T. Amo, S. Ohta, Y. Katsumata, K. Fukuda, K. Ishiwata, et al. 2011. Caloric restriction primes mitochondria for ischemic stress by deacetylating specific mitochondrial proteins of the electron transport chain. *Circ. Res.* 109:396–406. http://dx.doi.org/10.1161/CIRCRESAHA.111.243097

Sol, E.M., S.A. Wagner, B.T. Weinert, A. Kumar, H.S. Kim, C.X. Deng, and C. Choudhary. 2012. Proteomic investigations of lysine acetylation identify diverse substrates of mitochondrial deacetylase sirt3. *PLoS ONE*. 7:e50545. http://dx.doi.org/10.1371/journal.pone.0050545

Someya, S., W. Yu, W.C. Hallows, J. Xu, J.M. Vann, C. Leeuwenburgh, M. Tanokura, J.M. Denu, and T.A. Prolla. 2010. Sirt3 mediates reduction of oxidative damage and prevention of age-related hearing loss under caloric restriction. *Cell*. 143:802–812. http://dx.doi.org/10.1016/j.cell.2010.10.002

Tao, R., M.C. Coleman, J.D. Pennington, O. Ozden, S.H. Park, H. Jiang, H.S. Kim, C.R. Flynn, S. Hill, W. Hayes McDonald, et al. 2010. Sirt3-mediated deacetylation of evolutionarily conserved lysine 122 regulates MnSOD activity in response to stress. *Mol. Cell*. 40:893–904. http://dx.doi.org/10.1016/j.molcel.2010.12.013

Wallace, D.C. 2005. A mitochondrial paradigm of metabolic and degenerative diseases, aging, and cancer: a dawn for evolutionary medicine. *Annu. Rev. Genet.* 39:359–407. http://dx.doi.org/10.1146/annurev.genet.39.110304.095751

Wang, X., R.P. Rao, T. Kosakowska-Cholody, M.A. Masood, E. Southon, H. Zhang, C. Berthet, K. Nagashim, T.K. Veenstra, L. Tessarollo, et al. 2009. Mitochondrial degeneration and not apoptosis is the primary cause of embryonic lethality in ceramide transfer protein mutant mice. *J. Cell Biol.* 184:143–158. http://dx.doi.org/10.1083/jcb.200807176

Warburg, O. 1956. On respiratory impairment in cancer cells. *Science*. 124:269–270.

Weinert, B.T., S.A. Wagner, H. Horn, P. Henriksen, W.R. Liu, J.V. Olsen, L.J. Jensen, and C. Choudhary. 2011. Proteome-wide mapping of the *Drosophila* acetylome demonstrates a high degree of conservation of lysine acetylation. *Sci. Signal.* 4:ra48. http://dx.doi.org/10.1126/scisignal.2001902

Wittig, I., H.P. Braun, and H. Schägger. 2006. Blue native PAGE. *Nat. Protoc.* 1:418–428. http://dx.doi.org/10.1038/nprot.2006.62

Wood, J.G., B. Rogina, S. Lavu, K. Howitz, S.L. Helfand, M. Tatar, and D. Sinclair. 2004. Sirtuin activators mimic caloric restriction and delay ageing in metazoans. *Nature*. 430:686–689. http://dx.doi.org/10.1038/nature02789

Wu, Y.T., H.C. Lee, C.C. Liao, and Y.H. Wei. 2013. Regulation of mitochondrial F(o)F(1)ATPase activity by Sirt3-catalyzed deacetylation and its deficiency in human cells harboring 4977bp deletion of mitochondrial DNA. *Biochim. Biophys. Acta*. 1832:216–227. http://dx.doi.org/10.1016/j.bbadis.2012.10.002

Xie, H.B., and K.G. Golic. 2004. Gene deletions by ends-in targeting in *Drosophila melanogaster*. *Genetics*. 168:1477–1489. http://dx.doi.org/10.1534/genetics.104.030882

Xiong, Y., and K.L. Guan. 2012. Mechanistic insights into the regulation of metabolic enzymes by acetylation. *J. Cell Biol.* 198:155–164. http://dx.doi.org/10.1083/jcb.201202056

Yang, X.J. 2004. Lysine acetylation and the bromodomain: a new partnership for signaling. *BioEssays*. 26:1076–1087. http://dx.doi.org/10.1002/bies.20104

Yonamine, I., T. Bamba, N.K. Nirala, N. Jesmin, T. Kosakowska-Cholody, K. Nagashima, E. Fukusaki, J.K. Acharya, and U. Acharya. 2011. Sphingosine kinases and their metabolites modulate endolysosomal trafficking in photoreceptors. *J. Cell Biol.* 192:557–567. http://dx.doi.org/10.1083/jcb.201004098

Yoshino, J., K.F. Mills, M.J. Yoon, and S. Imai. 2011. Nicotinamide mononucleotide, a key NAD(+) intermediate, treats the pathophysiology of diet- and age-induced diabetes in mice. *Cell Metab.* 14:528–536. http://dx.doi.org/10.1016/j.cmet.2011.08.014

Zhai, R.G., Y. Cao, P.R. Hiesinger, Y. Zhou, S.Q. Mehta, K.L. Schulze, P. Verstreken, and H.J. Bellen. 2006. *Drosophila* NMNAT maintains neural integrity independent of its NAD synthesis activity. *PLoS Biol.* 4:e416. http://dx.doi.org/10.1371/journal.pbio.0040416

Zhao, S., W. Xu, W. Jiang, W. Yu, Y. Lin, T. Zhang, J. Yao, L. Zhou, Y. Zeng, H. Li, et al. 2010. Regulation of cellular metabolism by protein lysine acetylation. *Science*. 327:1000–1004. http://dx.doi.org/10.1126/science.1179689

Zhu, L.J., C. Gazin, N.D. Lawson, H. Pagès, S.M. Lin, D.S. Lapointe, and M.R. Green. 2010. ChIPpeakAnno: a Bioconductor package to annotate ChIP-seq and ChIP-chip data. *BMC Bioinformatics*. 11:237. http://dx.doi.org/10.1186/1471-2105-11-237